Breakaway oxidation of zirconium alloys exposed to steam around 1000 °C

Matthieu Le Saux, Jean-Christophe Brachet, Valérie Vandenberghe, Antoine Ambard, Raphaël Chosson

▶ **To cite this version:**

Matthieu Le Saux, Jean-Christophe Brachet, Valérie Vandenberghe, Antoine Ambard, Raphaël Chosson. Breakaway oxidation of zirconium alloys exposed to steam around 1000 °C. Corrosion Science, 2020, 176 (108936), pp.1-21. 10.1016/j.corsci.2020.108936 . hal-02924036

HAL Id: hal-02924036

https://ensta-bretagne.hal.science/hal-02924036

Submitted on 12 Mar 2021

HAL is a multi-disciplinary open access archive for the deposit and dissemination of scientific research documents, whether they are published or not. The documents may come from teaching and research institutions in France or abroad, or from public or private research centers.

L'archive ouverte pluridisciplinaire **HAL**, est destinée au dépôt et à la diffusion de documents scientifiques de niveau recherche, publiés ou non, émanant des établissements d'enseignement et de recherche français ou étrangers, des laboratoires publics ou privés.

Breakaway oxidation of zirconium alloys exposed to steam around 1000°C

M. Le Saux [a,b *], J.C. Brachet [a], V. Vandenberghe [a,c], A. Ambard [d], R. Chosson [e]

[a] *DES-Service de Recherches Métallurgiques Appliquées (SRMA), CEA, Université Paris-Saclay, F-91191 Gif-sur-Yvette, France*
[b] *Now at ENSTA Bretagne, UMR CNRS 6027, IRDL, F-29200 Brest, France*
[c] *Now at DES-Service d'Etudes Mécaniques et Thermiques (SEMT), CEA, Université Paris-Saclay, F-91191 Gif-sur-Yvette, France*
[d] *EDF R&D, MMC Department, avenue des Renardières, 77818 Moret-Sur-Loing, France*
[e] *Framatome, 10 rue Juliette Récamier, 69456 Lyon, Cedex 06, France*

Abstract
The breakaway oxidation of Zircaloy-4 and $M5_{Framatome}$ alloys oxidized in flowing steam around 1000°C was studied. The influences of oxidation temperature between 950 and 1050°C, one-side versus two-side oxidation and chemical variations around the nominal composition of $M5_{Framatome}$ were investigated. Breakaway oxidation is sensitive to the oxidation temperature, the material and the oxidation type. A phenomenological mechanism for breakaway oxidation is postulated on the basis of microstructural and microchemical analyses.

Keywords: Zircaloy-4; $M5_{Framatome}$; breakaway oxidation; high temperature; LOCA

1. Introduction

In some hypothetical accidental scenarios in nuclear Pressurized Water Reactors (PWR), such as LOss of Coolant Accidents (LOCA), fuel cladding tubes made of zirconium alloys can be exposed for a few minutes to steam at High Temperature (HT, up to 1200°C) before being cooled and then quenched in water by the emergency core cooling systems. Under steam at HT, zirconium alloys with no pre-existing oxide usually show a parabolic or sub-parabolic oxidation kinetics [1][2][3][4][5]. Furthermore, they generally do not absorb a significant amount of hydrogen [6][7] (however, recent results have shown a hydrogen uptake directly after exposure to steam at HT followed by a slight release of hydrogen [8]). Indeed, in those cases, the oxide is dense, adherent and protective with respect to hydrogen pickup. However, in some conditions, at temperatures between 600 and 1050°C typically, an increase of the oxidation rate and a hydrogen pickup is sometimes observed after an incubation period [3][4][5][9][10][11][12][13][14][15][16][17][18][19]. This transition is commonly called breakaway oxidation. The increase in the oxidation rate and the hydrogen pickup can then enhance deterioration of the mechanical properties of the cladding due to the embrittlement effects of oxidation and hydrogen [5][6][7][11][19][20][21][22]. This may be detrimental to the cladding integrity.

Previous results have shown that the breakaway oxidation of as-received low tin Zircaloy-4 and $M5_{Framatome}$[†] claddings occurs after an incubation time of a few thousands of seconds typically, depending on the study [4][5][11][23][25]. Furthermore, during in-service operation in PWR, an oxide layer grows on the cladding outer surface due to corrosion by the water environment (155 bar, ~300-340°C), and a fraction of the hydrogen released is absorbed by the cladding. It was obseved for low tin Zircaloy-4 and $M5_{Framatome}$ that the occurrence of breakaway oxidation

[*] Corresponding author.
Email address: matthieu.le_saux@ensta-bretagne.fr (M. Le Saux)
[†] $M5_{Framatome}$ is a registered trademark of Framatome or its affiliates, in the USA or other countries.

was not significantly modified by pre-hydriding up to 600 weight parts per million (wppm) [5] or by 10-13 µm-thick pre-oxides formed under water at 340-360°C [23].

Numerous factors are assumed to influence the breakaway oxidation and its incubation time: in particular, the oxidation temperature which is the first order parameter [9][10][12], but also the material, its fabrication process and its surface preparation [11][12][24][25]. The differences observed between some of the results reported in the literature illustrate this sensitivity. It was also observed that breakaway oxidation is affected by the testing conditions (composition of the oxidizing atmosphere, flow rate, …) [19][26]. This makes it difficult to compare the data reported in the literature obtained by using various facilities.

The results published by Leistikow and Schanz [9][10] in the 1980's for Zircaloy-4 alloy (with a tin content higher than the modern commercial ingots) showed that the incubation period to breakaway oxidation under steam is the shortest at 1000°C (around 20 min). Since then, most studies on the breakaway oxidation of zirconium alloys have been conducted at this temperature. Only scarce data were reported in the literature on the influence of temperature on the breakaway oxidation of modern zirconium alloys in steam [11][12][25]. In most of these papers, the determination of breakaway oxidation was based on the increase in the oxidation rate and visual examination of the oxide. Indeed, it was often observed that the outer surface of the oxide layer changed in colour after the breakaway oxidation transition, from dark grey or black to whitish, yellowish or pinkish depending on the alloy in particular. However, hydrogen pickup was often not provided, although it seems to be a more reliable feature to determine the incubation period to breakaway oxidation with accuracy. Therefore, it has been proposed to define the breakaway incubation period as the time required for the cladding to pickup 200 wppm [11]. Furthermore, a scalloped metal-oxide interface is commonly observed prior to breakaway oxidation. To the authors' knowledge, no quantitative characterization of this undulation of the metal-oxide interface was reported in the literature.

Breakaway oxidation undoubtedly results from a loss of protectiveness of the oxide layer during oxidation, with respect to oxygen and hydrogen transport to the metal-oxide interface. Nevertheless, the mechanisms that lead to it are not very well known yet, even though as soon as in the 1980's, Leistikow and Schanz [9][10] proposed a scenario, based on the fact that the phenomenon appeared for temperatures at which a phase transformation from the tetragonal phase to the monoclinic phase was likely to occur. The knowledge of the mechanisms at the origin of the breakaway oxidation seems however to be essential to correctly understand the phenomenon and to explain its sensitivity and the laboratory-to-laboratory variability sometimes observed.

This work focusses on the influences of three parameters on the breakaway oxidation of Zircaloy-4 and $M5_{Framatome}$ alloys when oxidized under flowing steam: effect of oxidation temperature around 1000°C, comparison between one-side and two-side oxidation, and impact of small variations around the nominal composition of five chemicals elements in $M5_{Framatome}$.

The materials and the experimental procedures used for this study are described in Section 2. The results are presented in Section 3. Breakaway oxidation was analysed on the basis of weight gains, hydrogen pickup and appearance of the oxide layer. What is referred to as weight gain in the paper is actually a mass gain but the term weight gain is commonly used in the field of this study. Oxide microstructure, undulation of the metal-oxide interface and microchemical partition were analysed for a selected number of samples oxidized at 1000°C, in order to

determine the potential links between these features and breakaway oxidation. A mechanism for breakaway oxidation is finally postulated in Section 4.

2. Materials and experimental procedures

2.1. Materials

The experiments were made on commercial stress-relieved annealed low tin Zircaloy-4 and fully recrystallized $M5_{Framatome}$ cladding tube samples, with an outer diameter and a thickness of 9.5 and 0.57 mm, respectively. Three batches of Zircaloy-4 and two batches of $M5_{Framatome}$ were tested. In this paper, the so-called batch 1 of Zircaloy-4 and batch 1 of $M5_{Framatome}$ refer to claddings elaborated in the early 2000's. Batches 2 and 3 of Zircaloy-4 and batch 2 of $M5_{Framatome}$ are more recent. In addition, tests were performed on samples from cladding tubes variants with chemical composition (various contents of Nb, Fe, O, S and Hf) around the nominal specifications of $M5_{Framatome}$. The chemical compositions of the materials are given in weight % (wt%) or wppm in Table 1. The samples were not pre-oxidized before the tests.

2.2. Oxidation in steam at high temperature

Oxidation tests were performed in pure steam (no carrier gas) at atmospheric pressure at 950, 975, 1000, 1025 and 1050°C, with holding times between 55 and 15000 s. Some of the samples were oxidized on both their outer and inner surfaces (two-side oxidation); in that case, 30 mm-long samples were used. Other samples, 150 mm-long, were oxidized on their outer surface only (one-side oxidation). To prevent steam from coming into contact with the cladding inner surface, end-caps in Zircaloy-4 were welded under secondary vacuum at both extremities. The oxidation of end-caps was included in the weight gain measurements. The oxidation behaviour was probably affected in the immediate vicinity of the welds but no detrimental effect was expected on the overall oxidation of the sample. Post-oxidation observations have shown that oxidation was uniform along the cladding sample (maximal variation of the oxide thickness of a few percent typically), including near the end-caps.

Oxidation at HT was carried out by using the DEZIROX 1 facility [5][6][27][22][23]. For one-side oxidation, the sample hanged from an alumina holder via a hole in the sample upper end-cap. For two-side oxidation, the bottom end of the sample was positioned on an alumina holder allowing free access of steam to both inner and outer surfaces of the sample. Steam was produced from an electrode-type steam generator. Steam flow was directed down through an alumina chamber. The steam flow rate normalized to the cross-sectional area of the steam chamber was about 70 mg/(cm^2·s), which was assumed to be sufficient to avoid steam starvation [9][28]. The samples were heated to the desired temperatures by using a vertical resistive furnace. The power to the furnace was controlled via a built-in thermocouple. The set-point temperature was fixed before testing using a rod equipped with type S (PtRh-Pt) thermocouples, inserted at the same position as the sample into the furnace. Furthermore, temperature benchmarks are regularly performed on specimens equipped with type S thermocouples spot-welded on their outer surface. The samples were inserted into the furnace once it was tuned and stabilized at the target isothermal temperature and flushed with steam for at least 1 hour. The samples reached the target temperature approximately 30 s after their introduction into the furnace (average heating rate of approximately 30°C/s). The oxidation time commenced when the sample was placed into the furnace. After isothermal holding, the samples were directly quenched in water down to room temperature.

The absence of temperature overshoot was verified. Temperature variation around the target temperature was lower than ±5°C. Temperature gradients were checked to be lower than 10°C along the samples.

Sample dimensions and weight were measured before and after testing with an accuracy of 10^{-3} mm for diameter and thickness, 10^{-2} mm for length and 0.1 mg for weight. The weight gain per unit surface area was deduced from these measurements.

2.3. Characterizations after oxidation at high temperature

Hydrogen content measurements were performed by an inert gas fusion thermal conductivity (hot extraction) technique (HORIBA EMGA-821 and LECO RH404 analysers) on samples extracted from the specimens oxidized at HT, at mid-length of the two-sided oxidized specimens and at about 1 cm from the lower end of the one-sided oxidized specimens. The hydrogen analyses were performed on samples including the oxide layers when not flaked off (spalled). Hydrogen is expected to be mainly located in the prior-β_{Zr} layer; α_{Zr}(O) and oxide layers contain only a small amount of hydrogen [22]. Thus, the hydrogen contents measured by keeping the oxide layers may slightly underestimate the hydrogen content within the metal. Two to four hydrogen content measurements were done for each sample, cut in small pieces which were randomly chosen so that 100-200 mg were used for each measurement. Hydrogen concentrates and diffuses very quickly in the β_{Zr} layer at HT. Furthermore, a significant volume of material, randomly chosen, was used for the hydrogen content measurements (about 300 to 800 mg, which is approximately equivalent to 3 to 8-mm-long rings). Thus, it is considered that the risk of missing hydrogen pickup due to local measurement is low.

It cannot be excluded that hydrogen pickup was promoted in the vicinity of the welds of end-caps of one-sided specimens. Furthermore, the end-caps were made in Zircaloy-4 with metallurgical and surface states different from those of the tubes. They clearly exhibited earlier breakaway oxidation and larger hydrogen pickup that the tubes. However, it was supposed that the hydrogen potentially absorbed at sample ends during oxidation at HT did not have time to diffuse very far, excepting eventually for the longest oxidation times tested. Comparative hydrogen content measurements were performed on samples taken at mid-length and on samples taken at 1 cm from the ends of $M5_{Framatome}$ tubes one-sided oxidized for 15000 s at 1000°C. The hydrogen contents measured were closed to each other. This showed that the hydrogen contents measured at 1 cm from the tube ends were representative of the hydrogen pick-up of the tube and did not exclusively result from the diffusion of hydrogen absorbed by the end-caps.

The hydrogen content absorbed during oxidation at HT was deduced from the difference between hydrogen contents measured after and before oxidation, in weight ppm (wppm). The hydrogen content of the samples two-sided oxidized was divided by a factor two approximately (ratio between the cladding outer diameter and the sum of its inner and outer diameters), to be able to compare it to the hydrogen content of one-sided oxidized samples, assuming that breakaway occurred at the same time at inner and outer surfaces and that the fractions of hydrogen then absorbed via both surfaces were the same.

Several layers can be observed after cooling in the samples oxidized at HT: an outer ZrO_2 oxide layer, an intermediate metallic layer of oxygen-stabilized α_{Zr} phase (hexagonal close-packed structure) called α_{Zr}(O) containing 2 to 7 wt% of oxygen, and a prior-β_{Zr} layer (with a typical Widmanstätten or parallel-lath structure morphology resulting from the transformation of the β_{Zr} phase (body-centered cubic structure) into the α_{Zr} phase, during quenching) or a two-phase

α_{Zr} + prior-β_{Zr} layer depending on the oxidation temperature and time. The microstructure and the thickness of the different layers were observed by microscopy on polished transverse cross-sections obtained from the middle part of selected samples that had been oxidized at HT. Optical microscopy was used to measure the oxide thickness (measurement uncertainty of a few microns) and to characterize the undulation of the metal-oxide interface. When the thickness of the oxide layer was expected to be low, a nickel coating was applied before imbedding and polishing the sample on its inner and outer surfaces in order to stabilize the oxide layer and minimize the end effects during polishing. As already done in [6], [23] and [27], Scanning Electron Microscopy (SEM) (mainly in back scattered electron mode) and a specific image analysis procedure were used to quantify the fractions of $\alpha_{Zr}(O)$ and prior-β_{Zr} across the cladding wall thickness. In the following, the so-called $\alpha_{Zr}(O)$ phase layer corresponds to the "continuous" $\alpha_{Zr}(O)$ phase layer containing more than 90% of $\alpha_{Zr}(O)$. The measurements of oxide and $\alpha_{Zr}(O)$ phase thicknesses were performed at two to four azimuthal locations per sample

Electron-Probe Micro Analysis (EPMA) (CAMECA SX100 electron microprobe) was conducted on polished transverse cross-sections of a selected number of samples to examine the distribution of chemical elements within the oxide and the metal.

In order to examine the morphology of the oxide layers, observations by Field Emission Gun (FEG) SEM were made on either polished transverse cross-sections of selected samples, fracture surfaces of samples failed by mechanical testing (ring compression, three-point bending or impact tests) at room temperature after oxidation and quenching, or fracture surfaces of oxide fragments broken off (spalled) during oxidation or quenching.

One should keep in mind that the observations were made after cooling down to room temperature. They were not necessarily representative of the state of the oxide at HT, before cooling: the oxide can be damaged during cooling, under the effect of internal stresses generated from phase transformations of the metal and the oxide [29], and from differences between the thermal coefficients of the different phases/layers constituting the oxidized cladding material [30].

3. Results

3.1. Influence of oxidation temperature

Weight gains measured for both Zircaloy-4 and $M5_{Framatome}$ two-sided oxidized at 950, 975, 1000, 1025 and 1050°C are shown in Fig. 1 and Fig. 2. Before the onset of breakaway oxidation, the higher the temperature, the faster the oxidation kinetics. Within the temperature range investigated, the pre-breakaway oxidation is slower for $M5_{Framatome}$ than for Zircaloy-4. It must be recalled that the oxidation kinetics of the two alloys are very close to one another above 1100°C [5][6][23].

3.1.1. Zircaloy-4

As shown in Fig. 1 (a), at 950°C, the evolution of weight gain as a function of time suggested a slight acceleration of the oxidation kinetics starting from about 9500 s. The oxide layers of the samples oxidized 5000 and 7500 s at 950°C were adherent to the metal after oxidation and quenching and their outer surface was homogeneously smooth and black (Fig. 3). The samples oxidized 9500 and 15000 s at this temperature showed heterogeneous, whitish/greyish on the outer surface, crazed/cracked and locally delaminated and spalled. No hydrogen pickup was observed for oxidation times between 5000 and 9500 s. As shown in Fig. 1 (b), a significant

hydrogen pickup was measured after 15000 s. These results suggested that the incubation time needed for breakaway oxidation of Zircaloy-4 at 950°C was between 9500 and 15000 s (probably closer to 9500 s), for a weight gain of approximately 8-10 mg/cm^2.

The oxidation kinetics of Zircaloy-4 accelerated from 7500 s at 975°C (Fig. 1 (a)). After 3000 and 5000 s at this temperature, the oxides appeared to be homogeneously smooth and black and adhered to the substrate (Fig. 3). Whitish areas were observed locally on the outer surfaces after 7500 and 9500 s at 975°C. After 15000 s, the oxide was crazed/cracked and completely whitish. A significant hydrogen pickup was measured beyond 7500 s (Fig. 1 (b)). It increased in the course of oxidation. Hydrogen pickup was negligible for shorter oxidation times. The results thus revealed a breakaway oxidation time between 5000 and 7500 s at 975°C, corresponding to a weight gain between 8 and 11 mg/cm^2.

The weight gains and hydrogen pickups obtained at 1000°C are a little scattered (Fig. 1). An acceleration of the oxidation kinetics was observed from about 5000 s at 1000°C. Visual examination after quenching revealed a change in appearance: the outer oxide surface which appeared to be lustrous black for shorter oxidation times became whitish and crazed (Fig. 3). Hydrogen pickup was insignificant when the oxidation was shorter than 5000 s but significant beyond. According to these results, consistent with those reported in [5][11][23], breakaway oxidation of low tin Zircaloy-4 never occurred before about 5000 s at 1000°C, for a weight gain of 13-14 mg/cm^2.

It seemed likely that the oxidation kinetics got faster from an oxidation time ranging between 9500 and 15000 s at 1025°C (Fig. 1). The weight gains measured after 9500 or 15000 s at 1025°C were smaller than those obtained for the same oxidation times at 1000°C because accelerated oxidation took place sooner at 1000°C. While the oxides formed on samples oxidized during less than 9500 s at 1025°C were homogeneously black and adherent to the metal, they appeared to be heterogeneous, whitish coloured, veined and crazed/cracked after 15000 s oxidation. Hydrogen pickup was low until 9500 s at 1025°C but significant after 15000 s. The breakaway oxidation time at 1025°C was between 9500 and 15000 s, corresponding to a weight between 25 and 34 mg/cm^2.

At 1050°C, neither acceleration of the oxidation kinetics nor hydrogen pickup were evidenced for the oxidation times tested here (Fig. 1). Furthermore, the outer surface of the specimens was homogeneously black (Fig. 3). Thus, the results did not show any sign of breakaway oxidation at 1050°C for oxidation times up to 15000 s. After 9500 and 15000 s oxidation at this temperature and quenching, the oxide outer surface showed a veined appearance in some areas (Fig. 3). This may indicate that the oxide peeled off locally (without having spalled) under the effects of internal stresses generated during quenching [30]. As expected, the sample oxidized 15000 s at 1050°C failed during quenching due to the very high oxidation level achieved: Equivalent Cladding Reacted value (ECR, *i.e.* total thickness of cladding metal that would be converted to oxide if all the oxygen absorbed by and reacted with the cladding were converted to stoichiometric ZrO_2) of approximately 60% according to the measured weigh gain and the sample dimensions.

Fig. 4 shows the incubation time needed for breakaway oxidation as a function of the oxidation temperature. Data from the literature are reported in this figure for comparison. It must be pointed out that breakaway oxidation time for a given oxidation temperature can vary of several hundreds or even several thousands of seconds from one study to another and from one batch of material to another. The results presented herein show that breakaway oxidation of low tin

Zircaloy-4 occurs for oxidation times shorter than 15000 s at 950, 975, 1000 and 1025°C. The incubation time is the lowest at 1000°C and increases when one deviates from this temperature. This general trend is consistent with those that could be drawn from the data in the literature, although there is significant deviation on incubation times in some cases. No breakaway oxidation has been evidenced at 1050°C for oxidation times up to 15000 s to the authors' knowledge. As shown in Fig. 4, the higher the oxidation temperature between 950 and 1025°C, the larger the weight gain at which breakaway oxidation occurs: this weight gain is nearly the same at 950 and 975°C, a little larger at 1000°C and significantly higher at 1025°C.

3.1.2. M5$_{Framatome}$

M5$_{Framatome}$ from batch 2 did not show any sign of breakaway oxidation at 950 and 975°C for oxidation times up to 15000 s (Fig. 2 and Fig. 3).

No clear acceleration of weight gain (Fig. 2 (a)), significant hydrogen pickup (Fig. 2 (b)) or noticeable change in appearance (Fig. 3) were evidenced either after two-side oxidation at 1000°C, for oxidation times up to 15000 s (and weight gains up to about 11 mg/cm^2). Optical microscopy observations of cross-sections of samples oxidized 5000 and 15000 s at this temperature confirmed that the oxide thickness was uniform on average (however, there were local variations in oxide thickness since the metal-oxide interface appeared scalloped), similar at the inner and outer surfaces and consistent with the measured weigh gains. These results showed longer oxidation times to breakaway oxidation than those previously reported [5][23], which were about 5000 s at 1000°C (weight gain of 8-9 mg/cm^2). While the oxidation tests were done using the same facility, there are some differences, such as one-side oxidization as done in the tests presented in [5][23] versus two-side oxidation in the present study. These differences are further discussed in Section 3.2, where results of one-side and two-side oxidations are compared.

The results obtained did not show any marked acceleration of the oxidation kinetics at 1025°C for times up to 15000 s (Fig. 2 (a)). The oxide layers formed at this temperature appeared relatively homogeneous without crazing, cracking or spalling. However, the colour of the oxide outer surface gradually became paler as the oxidation time increased: it appeared black/dark grey after 5000 s and light grey after 15000 s. The material did not absorb very significant amount of hydrogen for the oxidation times tested (Fig. 2 (b)). Nevertheless, a slight hydrogen pickup (approximately 60 wppm) was measured after 15000 s oxidation, which may suggest that breakaway oxidation has just occurred. So, there was no clear evidence of breakaway oxidation of M5$_{Framatome}$ at 1025°C for times up to 15000 s or else it occurred at an oxidation time close to 15000 s, for a weight gain around 15 mg/cm^2.

There was a slight lightening (whitening) of the oxide surface from 9500 s oxidation and protrusions were observed after 15000 s oxidation at 1050°C (Fig. 3), but no noticeable acceleration or hydrogen pickup and thus no breakaway oxidation were evidenced.

There are very few data in the literature on the breakaway oxidation of M5$_{Framatome}$. No transition in oxidation kinetics was observed by Große [17] during two-side oxidation at 1000°C for 21600 s. This suggests that breakaway oxidation did not occur but data on hydrogen pickup would have been useful to confirm it. It must be noted that the oxidation kinetics reported in [17] was slightly slower than that observed during the present study, and a maximal weight gain of about 10 mg/cm^2 was achieved. No hydrogen pickup was reported in [11] after 3450 and 4100 s (weight gain of about 10.8 mg/cm^2) two-side oxidation of M5$_{Framatome}$ in steam at 1000°C. Despite the absence of significant acceleration of the oxidation kinetics, a hydrogen

pickup higher than 550 wppm was measured by Steinbrück *et al.* [25] for $M5_{Framatome}$ two-sided oxidized for 10800 s at 1000°C. It must be pointed out that the oxidation kinetics measured by Steinbrück *et al.* before breakaway oxidation was nearly two times faster than that obtained here. Considering the values of weight gain obtained, the hydrogen pickups reported in [11] and [25] are more or less consistent with those measured within the current study.

3.2. Comparison of one-side and two-side oxidations at 1000°C

Two-side oxidation is used by most laboratories to study breakaway oxidation of cladding tubes. The results presented in Section 3.1 were obtained from two-side oxidation tests. Nevertheless, one-side oxidation is sometimes used [5][19][23]. The results presented in the previous Section did not show breakaway oxidation for $M5_{Framatome}$ at 1000°C for times up to 15000 s while previous results obtained using the same facility showed breakaway oxidation after about 5000 s [5]. One-side and two-side oxidation tests were performed at 1000°C on the same batches of materials and facility to evaluate whether or not this deviation was due to the use of one-side and two-side oxidations. Some of the results of one-side oxidation tests were already presented in [5] and [23].

Three batches of low-tin Zircaloy-4 were used. As shown in Fig. 5, results close to one another were obtained after one-side oxidation and two-side oxidation for the three batches of low-tin Zircaloy-4, showing that breakaway oxidation of Zircaloy-4 is not very sensitive to these factors. However, it must be noted that the oxide layer did not spall during quenching after two-side oxidation as long as 15000 s while it did, partially (delamination) or completely, after one-side oxidation longer than 5000 s. This could be attributed to the internal stresses generated during cooling (due to phase transformations of the metal and the oxide and to differences between the thermal coefficients of the different phases/layers) [30] which may be different after one-side oxidation and two-side oxidation: it may be assumed that the stress levels are higher after one-side oxidation.

The results obtained for two batches of $M5_{Framatome}$ are shown in Fig. 6. In this figure, batch 1 is the one used for the tests performed in the early 2000's and presented in [5]. In the case of two-side oxidation, the values of weight gain and hydrogen pickup measured for the two batches after 15000 s oxidation are not far from one another. Similar weight gains were obtained for one-side and two-side oxidation at 1000°C for 5292 s, without manifestation of breakaway oxidation. After 9500 and 15000 s-long oxidation, the samples one-sided oxidized showed higher weight gains than the samples two-sided oxidized. However, metallographic examination revealed that this excess in weight gain was due to faster oxidation of the end-caps, made in Zircaloy-4 and clearly showing breakaway oxidation in these conditions. Indeed, the weight gain of end-caps is included in the weight gain measurement for one-sided oxidized samples. Although they also exhibited a homogeneous, black and adherent oxide, samples from the more recent batch 2 absorbed 120 and 250-500 wppm hydrogen during one-side oxidation for respectively 9500 and 15000 s, while no hydrogen pickup was measured after two-side oxidation in the same conditions. As discussed in Section 2.3, this hydrogen pick-up is not expected to come only from the diffusion of the hydrogen absorbed by the sample end-caps. The samples from batch 1 one-sided oxidized during 15000 s at 1000°C during the same test campaign showed features of post-breakaway oxidation, in agreement with the results presented in [5]. These results suggested that, in the case of $M5_{Framatome}$ cladding tubes, the results of breakaway oxidation tests at 1000°C may be different whether the inner surface of the cladding was oxidized in addition to the outer surface or not. This may be related to oxidation-induced stresses different in the cases of one-side oxidation and two-side oxidation. These stresses are likely to have an effect on the stability of the tetragonal structure of zirconia [31]. So, in the

case of two-side oxidation, no breakaway oxidation was detected at 1000°C for oxidation times up to 15000 s for either batches of $M5_{Framatome}$ tested.

3.3. Hydrogen pickup fraction at 1000°C

The "instantaneous" hydrogen pickup fraction reduced to the outer surface, f_{Ha}, has been defined as the ratio of the hydrogen absorbed by the material over the total hydrogen generated during the oxidation over a time period $[t; t+\Delta t]$. It was calculated as follows [32]:

$$f_{Ha} = 10^{-6} \frac{M_O}{2M_H} \frac{\widehat{m}^{t+\Delta t} C_H^{t+\Delta t} - m^t C_H^t}{\widehat{m}^{t+\Delta t} - m^t} \quad (1)$$

M_O and M_H are the atomic masses of oxygen and hydrogen respectively. m^t and C_H^t are respectively the total mass and the hydrogen content reduced the cladding outer surface of the sample oxidized for a duration t at 1000°C. The measurements at the different time periods were performed on separate samples. The (slight) differences in mass and surface area between the samples oxidized for t and $t+\Delta t$ durations were taken into account by readjusting the mass of the sample oxidized for $t+\Delta t$, as illustrated in Fig. 7. $\widehat{m}^{t+\Delta t}$ in the equation above is therefore the mass that the sample oxidized for $t+\Delta t$ would have had if its initial mass and surface area were the same as those of the sample oxidized for a duration t:

$$\widehat{m}^{t+\Delta t} = m_0^t + S_0^t \frac{m^{t+\Delta t} - m_0^{t+\Delta t}}{S_0^{t+\Delta t}} \quad (2)$$

where $S_0^{t+\Delta t}$, $m_0^{t+\Delta t}$ and $m^{t+\Delta t}$ are respectively the actual values of the initial surface area exposed to steam, the initial mass and the final mass of the sample oxidized for $t+\Delta t$. S_0^t and m_0^t are the surface area and the initial mass of the sample oxidized for a duration t. f_{Ha} can be considered as an "instantaneous" value of the hydrogen pickup fraction, averaged over a range of oxidation times, more or less extended depending on the time increment between the tests performed. Fig. 8 shows the "instantaneous" hydrogen pickup fractions evaluated for Zircaloy-4 either one-sided or two-sided oxidized and $M5_{Framatome}$ one-sided oxidized at 1000°C. Error bars in this figure correspond to the ranges of oxidation times over which the average "instantaneous" hydrogen pickup fractions were determined. Although they were approximate, the results showed that both alloys absorbed a large fraction of hydrogen at the onset of breakaway oxidation, up to at approximately 50%. The values reported here are average values over oxidation time ranges of several hundred seconds in most cases. It can therefore be assumed that the truly "instantaneous" hydrogen pickup fractions, *i.e.* those that would have been determined over very small oxidation time increments, were even higher than 50%. The fraction of hydrogen absorbed then decreased and stabilized around 10-30% during further oxidation. Hydrogen pickup was thus associated with a transition.

3.4. Sensitivity to chemical composition variations for $M5_{Framatome}$ at 1000°C

In order to study the sensitivity of breakaway oxidation of $M5_{Framatome}$ to the content of alloying elements and main impurities, materials with various chemical compositions around the nominal composition of $M5_{Framatome}$ were one-sided oxidized at 1000°C for 3270, 5292 and 9500 s, then directly water quenched. One test of 3270 s and two tests of 5292 s and 9500 s were performed for each material. Hydrogen content measurements were performed on the specimen with the highest weight gain.

The results are shown in Fig. 9 together with those obtained on standard $M5_{Framatome}$, already presented in [5] and [23]. After 3270 s at 1000°C, the weight gains measured for the various chemical variants were close to one another, and no significant hydrogen pickup was measured (it remained below 100 wppm). Weight gains measured after 5292 and 9500 s deviated from the sub-parabolic oxidation kinetics observed for shorter oxidation times. The acceleration of the oxidation kinetics after approximately 5000 s at 1000°C was associated with a significant

hydrogen pickup. The quantity of hydrogen absorbed by the material increased during oxidation. After 5292 s, weight gains and hydrogen pickups were more widespread than for shorter oxidation. The dispersion was larger after 9500 s. As shown in Fig. 10, the quantity of hydrogen absorbed by the materials and the weight gains were consistent. No significant spalling of the oxide was observed after 3270 s at 1000°C and quenching, for all tested materials. Oxide spalling appeared during quenching after 5292 s oxidation. More significant and scattered spalling was observed for longer oxidation. Thus, the results showed that the pre-breakaway oxidation kinetics and the time needed for the onset of breakaway oxidation were not significantly modified by chemical composition variations around the nominal composition of $M5_{Framatome}$: considering that breakaway oxidation corresponded to an increase in the oxidation rate and to an hydrogen pickup higher than 100 wppm (for one-side oxidation), the breakaway oxidation time was in all cases around 5000 s, corresponding to a weight gain of about 10 mg/cm^2. After the onset of breakaway oxidation, some differences were observed on weight gains and hydrogen uptakes but, given the dispersion of the results, no clear trend in the effect of the chemical elements can be evidenced.

3.5. Microstructural observations

As discussed in Section 3.1, the time needed for the onset of breakaway oxidation is the lowest at 1000°C, at least for Zircaloy-4. Therefore, microstructural observations were carried out on a selected number of Zircaloy-4 (batch 1) and $M5_{Framatome}$ (batch 1) samples one-sided oxidized at 1000°C and water quenched. In particular, the following characteristics were studied: oxide and $\alpha_{Zr}(O)$ phase thicknesses, undulation of the metal-oxide interface, oxide microstructure and microchemical partitioning within the oxide and the underlying metal.

3.5.1. Oxide thickness and undulation of the metal-oxide interface

The oxide layer of Zircaloy-4 and $M5_{Framatome}$ samples respectively oxidized 5000 s and 5292 s at 1000°C has completely spalled during quenching. For shorter oxidation, the oxide remained adherent to the metal. For longer oxidation, the outer part of the oxide layer has delaminated and spalled. Fig. 11 shows the thicknesses of the oxide layer and the $\alpha_{Zr}(O)$ layer before the onset of breakaway oxidation. The ratio determined from data reported in [7] and [23] for oxidation performed at 1100, 1200 and 1250°C in the same facility are included in Fig. 11 for comparison. The thickness of the $\alpha_{Zr}(O)$ layer provides information on the quantity of oxygen having diffused through the metallic substrate (the amount of oxygen diffusing within the underlying β_{Zr} phase being low by comparison). On the one hand, in the case of Zircaloy-4, the ratio between the thicknesses of the $\alpha_{Zr}(O)$ layer and the oxide layer was nearly one. This tendency was similar to those obtained at 1100, 1200 and 1250°C either for Zircaloy-4 or $M5_{Framatome}$. One the other hand, in the case of $M5_{Framatome}$, the $\alpha_{Zr}(O)$ layer was significantly thicker (by approximately a factor 3 after 3270 s at 1000°C) than the oxide layer.

The oxide thickness and the undulation of the metal-oxide interface were characterized from optical micrographs of polished cross-sections (mainly perpendicular to the tube axis) by using an image analysis procedure. A dozen of pictures were taken for each sample along the tube circumference, so that at least half of the circumference was examined. Fig. 12 shows the average thickness of the oxide remaining at the sample surface after quenching and the total oxide thickness expected. This last quantity was evaluated by using the following relationships between the oxide thickness t_{ZrO2} (in µm) and the weight gain w (in mg/cm^2): $t_{ZrO2} = 5.0758w$ for Zircaloy-4 and $t_{ZrO2} = 3.2543w$ for $M5_{Framatome}$. These relationships were established from the pre-breakaway oxidation data shown in Fig. 11 for which the oxide did not spalled (oxidation times up to 3270 s, *i.e.* weight gain lower than or equal to 10.9 mg/cm^2 and 6.7 mg/cm^2 for Zircaloy-4 and $M5_{Framatome}$, respectively). The factor between t_{ZrO2} and w is

significantly lower for M5 than for Zircaloy-4. This shows that a larger fraction of the oxygen having reacted with the material has diffused through the metallic substrate in the case of $M5_{Framatome}$. The fraction of oxygen having contributed to the growth of zirconia was smaller, as illustrated in Fig. 11 shows that the oxide layer was thicker for Zircaloy-4 than for $M5_{Framatome}$, for a given oxidation time.

The undulation of the metal-oxide interface can be characterized at various scales, from a few tens of nanometers to a few tens of microns. The undulations examined here were those that could be observed at low magnification (x10 in the present study; Fig. 13). It was considered that an undulation corresponded to a local variation of oxide thickness larger than 10% of the average oxide thickness. The local oxide thickness was measured from optical micrographs every 4 µm in average, by scanning one half section of the samples (a dozen of images were analysed per half section). The amplitude and wavelength of the undulations at the metal-oxide interface were determined from these measurements (Fig. 14). The results are shown in Fig. 15, where error bars represent the standard deviation on the measurements. They are an indicator of the homogeneity of the features of undulation. Besides, the length of the metal-oxide interface l was measured. The elongation of the metal-oxide interface due to undulation relatively to an interface of length l_0 that would not be wavy was then calculated: $l/l_0 - 1$. The results are illustrated in Fig. 16. For Zircaloy-4 as for $M5_{Framatome}$, undulation of the metal-oxide interface at the microscale appeared after approximately 15-20 min at 1000°C, for oxide thicknesses of about 30 and 15 µm for Zircaloy-4 and $M5_{Framatome}$, respectively (or respective weight gains of about 6 et 4 mg/cm^2).

In the case of Zircaloy-4, before the onset of breakaway oxidation, the amplitude of undulation continuously increased in the course of oxidation, more or less proportionally to the average oxide thickness (Fig. 15): the ratio between these two quantities remained around 20-30%. However, the wavelength of the undulation did not evolve much. The amplitude of undulation was the highest after 5000 s at 1000°C (breakaway oxidation time, after which the oxide layer has completely spalled during quenching), *i.e.* for a weight gain of approximately 10 mg/cm^2 and an expected oxide thickness of about 50 µm (Fig. 12). The amplitude was significantly smaller after 7500 s oxidation (16 mg/cm^2 weight gain and 80 µm expected oxide thickness). Standard deviation was high, revealing a certain variability of the undulation amplitude and distribution. The elongation of the metal-oxide interface due to undulation first increased during oxidation up to 3270 s to reach about 20% and then decreased (Fig. 16).

In the case of $M5_{Framatome}$, once the undulations have appeared, their amplitude first rapidly increased during oxidation but did not evolve much afterwards (Fig. 15), to remain close to 5 µm (10-20% of the average oxide thickness). The amplitude of undulation was smaller than that obtained for Zircaloy-4, expect after 7500 s oxidation for which they were close to one another. Although if progressively increased during oxidation, the wavelength of undulation was smaller than in the case of Zircaloy-4. Furthermore, as illustrated by the smaller standard deviations, micro-scale undulations at the metal-oxide were less variable and more homogeneously distributed. The elongation of the metal-oxide interface due to undulation was approximately 5% and was thus significantly smaller than that determined for Zircaloy-4 (Fig. 16).

Finally, it must be pointed out that the wavelength of the undulation of the metal-oxide interface and the size of the $\alpha_{Zr}(O)$ grains near this interface had the same order of magnitude.

3.5.2. Morphology of the oxide layers

Fig. 17 (a) illustrates typical observations of cross-sections of Zircaloy-4 and $M5_{Framatome}$ samples oxidized about 30 min at 1000°C (*i.e.* before the onset of breakaway oxidation). They revealed micro-cracks parallel to the metal-oxide interface and interfacial decohesion between the oxide and the metallic substrate near the regions of delayed oxidation (see Fig. 14). Such cracks were not detected for shorter oxidation times. Longer and wider cracks were observed for longer oxidation times. A network of cracks parallel to the metal-oxide interface was observed at about 20 µm from the interface within the oxide sublayer that has remained adherent on $M5_{Framatome}$ samples oxidized approximately 15000 s at 1000°C (Fig. 17 (b)). In the samples oxidized 5000 s, cracks perpendicular to the outer surface were detected after quenching in the delayed oxidation regions of the oxide sublayer still adherent to the metal (separation of oxide crystallites). Micrographs revealed cracks perpendicular to the metal-oxide interface within the $\alpha_{Zr}(O)$ layer, mainly in the advanced oxidation regions. These cracks probably formed during cooling as a result of the internal stresses associated with the phase transformations and the mismatch of the thermal expansions of the different phases/layers constituting the cladding material oxidized at HT [30]. However, the preferential location of these cracks may illustrate that these internal stresses are heterogeneous and that this heterogeneity is related to the undulation of the metal-oxide interface.

Fig. 18 and Fig. 19 give examples of micrographs of the fracture surface of samples mechanically tested after oxidation and cooling. The micrographs focus on the zirconia layer (mainly intergranular brittle fracture). Outer and inner surfaces of spalled oxide fragments are also shown in some cases. The inner surface of the spalled oxide sublayer (oxidation of 5000 s and more) showed an egg-box-like structure (three-dimensional representation of the undulation of the metal-oxide interface observed on samples cross-sections).

Pre-breakaway oxide layers (oxidation times shorter than 5000 s) formed at 1000°C showed a columnar structure. The crystallites were mainly oriented perpendicular to the metal-oxide interface. The development of such a microstructure is primarily driven by the minimization of the stresses within the oxide [33]. Overall, a similar columnar structure was observed for the oxide layers having completely spalled during quenching after 5000 s and 5292 s at 1000°C, for Zircaloy-4 and $M5_{Framatome}$ respectively (Fig. 18 (a)). Cracks perpendicular to the oxide surface (called radial cracks) were evidenced within the oxide in the advanced oxidation regions.

In the case of Zircaloy-4 oxidized for 7500 s at 1000°C (Fig. 18 (b)), crystallites of the oxide sublayer still adherent to the metal after quenching were oriented perpendicular to the undulated interface between the spalled oxide sublayer and the residual adherent oxide sublayer. This orientation may result from preferential growth directions of crystallites according to the heterogeneous stress field near the undulated metal-oxide interface, or from strong deformation of oxide grains during oxidation or quenching. Crystallites of the oxide sublayer adherent to the metal were oriented perpendicular to the outer oxide surface, without clear link with undulation of the interface between spalled and adherent oxide sublayers. Examination of the inner surface (egg-box-like structure) and the outer surface of the spalled oxide sublayer revealed a network of radial cracks in front of areas where the oxide was the thicker. A few radial cracks were also evidenced within the adherent oxide sublayer.

In the case of $M5_{Framatome}$ oxidized for 9500 s at 1000°C (Fig. 19 (a)), oxide crystallites appeared less columnar and wider within the spalled oxide sublayer than within the one that has remained

adherent to the metal. Furthermore, micro-cracks parallel to the metal-oxide interface and radial cracks were observed within the oxide sublayer having broken off.

After 14551 s oxidation at 1000°C and quenching (Fig. 19 (b)), the oxide sublayer formed on $M5_{Framatome}$ that has remained adherent exhibited more numerous cracks and intergranular micro-pores, and shorter and wider crystallites in delayed oxidation regions (where decohesion was observed) than in advanced oxidation regions. Cracks parallel to the metal-oxide interface were also observed.

In summary, Fig. 20 illustrates the typical post-breakaway oxidation microstructure of the oxide and the underlying metal. After quenching, the spalled sublayer of post-breakaway oxides and the adherent sublayer of these oxides in the delayed oxidation regions exhibited more numerous cracks and micro-pores, and shorter and wider crystallites, than either the pre-breakaway oxide layers (oxidation times lower than approximately 5000 s) or the advanced oxidation regions of the sublayer of post-breakaway oxides that has remained adherent. Finally, one should keep in mind that the observations were made after cooling and mechanical testing, during which some of the pores and cracks that have been observed may have formed.

3.5.3. Distribution of alloying elements

Chemical microanalysis was performed by EPMA on transverse cross-sections of Zircaloy-4 and $M5_{Framatome}$ samples oxidized 3270 and 7500 s at 1000°C and then quenched. In the case of Zircaloy-4, iron and chromium were mainly concentrated into the prior-β_{Zr} layer and the concentration of tin was higher in the $\alpha_{Zr}(O)$ than in the prior-β_{Zr} layer, as expected after oxidation at 1000°C (but not for higher oxidation temperatures) as discussed in [34]. Fig. 21 and Fig. 22 show that tin was heterogeneously distributed within the oxide and the underlying $\alpha_{Zr}(O)$ phase, with a certain microchemical continuity on both sides of the metal-oxide interface. Tin concentration within the $\alpha_{Zr}(O)$ layer varied between approximately 0.8 and 1.6 wt%, around the tin mean content of the alloy (1.3 wt%) (Fig. 21). At 1000°C, diffusion of tin is slower than that of other alloying elements and slower by far in α_{Zr} than in β_{Zr} [35][36]. This explains the partition of tin observed in the metal. The average periodicity of fluctuations in tin concentration was about 30 µm for both 3270 s and 7500 s oxidation times. This distance of diffusion was consistent with the free mean path calculated for tin at 1000°C [35][36]. The average wavelength of the undulation of the metal-oxide interface was of the same order of magnitude (Fig. 15 (b)). It appeared that undulation of the metal-oxide interface and distribution of tin within the oxide and the metal in the vicinity of this interface were correlated.

The ratio between the atomic concentrations of tin and zirconium was nearly the same at both sides of the metal-oxide interface (Fig. 22). Similar tin concentration within the metallic substrate was measured in average for both 3270 s and 7500 s oxidation times. It appeared that the tin concentration within the oxide layer formed after 3270 s at 1000°C was slightly lower in the outer part of the layer (about 0.6 wt% or 0.2 at% in average) than near the metal-oxide interface (approximately 0.9 wt% or 0.3 at.%).

A “line” very rich in tin parallel to the metal-oxide interface was observed at a dozen of microns from the interface within the oxide layer formed after 7500 s at 1000°C. In this “line”, tin concentration was higher than 13 wt% (maximal value measured with a spatial resolution of 1 µm), oxygen content was the same as in the rest of the oxide and zirconium content was slightly lower. Tin concentration was lower between the “tin line” and the outer surface of the remaining oxide sublayer than below the “tin line”. This “line” rich in tin may have resulted from the accumulation of tin precipitates (tin diffuses more slowly than oxygen within the oxide and the

metal, and the solubility of tin in the oxide is very low) until these precipitates were molten when the tin concentration was high enough. This type of "line" rich in tin has already been observed for oxidation performed at other temperatures [37][38]. It seemed that it did not have a significant effect on the overall oxidation kinetics.

In the case of $M5_{Framatome}$, as illustrated in Fig. 23, the prior-β_{Zr} layer was enriched in niobium (β_{Zr}-stabilizer) after oxidation at 1000°C. As observed for tin in Zircaloy-4, the distribution of niobium in the oxide and the $\alpha_{Zr}(O)$ layer of $M5_{Framatome}$ samples oxidized for 3270 and 7500 s at 1000°C was heterogeneous (niobium depleted zones alternated with zones enriched in niobium), with a microchemical continuity on either side of the metal-oxide interface. The partition of niobium in the metal is related to the diffusion of niobium which is slower than that of other elements and slower in α_{Zr} than in β_{Zr}: as already reported in [41], in zirconium alloys containing niobium, thin layers of β_{Zr} enriched in niobium grow together with coarser layers of $\alpha_{Zr}(O)$ depleted in niobium during oxidation at HT. As shown in Fig. 23, the niobium concentration within the oxide and the underlying metallic layer varied (around 0.9 wt% average value) between approximately 0.1 and 14 wt% (highest value measured with a 1 µm spatial resolution) with a modulation period of about 20 µm. This wavelength was consistent with the free mean path estimated for niobium [35][36]. The amplitude of modulation was larger for niobium in $M5_{Framatome}$ than for tin in Zircaloy-4. Undulation of the metal-oxide interface seemed to be correlated with fluctuation of niobium on both sides of the metal-oxide interface.

The amplitude of modulation in niobium concentration within the oxide was smaller after 3270 s than after 7500 s at 1000°C. However, it was nearly the same within the metallic substrate for both oxidation times and was almost similar within the oxide and within the metallic substrate of the sample oxidized for 7500 s.

In the two-phase $\alpha_{Zr}(O) + \beta_{Zr}$ layer, at a few tens of microns from the metal-oxide interface, the niobium concentration diminished when moving away from this interface, proportionally to the inverse of the oxygen concentration. The niobium content was almost zero in the metal when the local oxygen content was approximately 2-2.5 wt%. In the oxide, zones enriched in niobium (niobium concentration higher than 1 wt%) represented about 15% of the whole oxide surface. In the two-phase $\alpha_{Zr}(O) + \beta_{Zr}$ layer, the surface fraction of the phase enriched in niobium (concentration above 1 wt%) and depleted in oxygen (concentration lower than 1.9 wt%) was between 10 and 20%; this fraction logically increased when going away from the metal-oxide interface.

4. Discussion

In the 1980's, Leistikow and Schanz [9][10] suggested a mechanism of breakaway oxidation at HT. However, to date, there is still no consensus in the precise mechanisms responsible for the phenomenon.

4.1. Morphology, porosity and cracking of the oxide

The oxidation kinetics and the hydrogen pickup are linked to the characteristics of the oxide: grains morphology, cohesion between grains, density and location of pores (resulting from clustering of vacancies for example) and cracks. The results presented above have shown that breakaway oxidation at HT is associated with both a change in the oxidation kinetics from sub-parabolic to nearly linear and a high hydrogen pickup fraction (several tens of percent). Thus, breakaway oxidation is related to a loss of protectiveness of the oxide layer in the course of oxidation. The examinations presented in Section 3.5, performed after oxidation at 1000°C and

quenching (the microstructure of the oxide was probably modified during quenching), showed that this loss of the protectiveness of the oxide layer can be related to the numerous cracks and micro-pores found after breakaway oxidation.

Before the onset of breakaway oxidation, dissociation of water and reduction/recombination of hydrogen may occur at the outer surface or within the "dense" existing oxide but far from the interface with the metal, so that the potential access of hydrogen to the metal (by solid state diffusion) would be limited. The amount of hydrogen at the metal-oxide interface would remain too low for the metal to absorb hydrogen. At this stage, the hydrogen content in the oxidized material would remain low in average, a few to a few tens of wppm typically. However, if steam is injected at HT on the metal with no pre-oxide (formed before or during heating to HT), a transitory hydrogen absorption may occur before a protective oxide layer has formed [8]. Additionally, based on the authors' knowledge, it must be mentioned that such transitory hydrogen uptake may also depend on the outer steam flux, a potential brief temperature overshoot...

At the onset of breakaway oxidation, it may be assumed that dissociation of water and reduction/recombination of hydrogen mainly take place at the vicinity of the metal-oxide interface. This presupposes that steam has access to the vicinity of the metal-oxide interface through a network of open pores and/or interconnected cracks in the oxide (transport in the gas phase). This network of interconnected defects may act as a "hydrogen pump" [8][39]: because of the oxidation of the metal, the partial pressure of gaseous hydrogen in pores and cracks near the metal-oxide interface would increase, leading to an additional hydrogen pickup, if it is assumed that the hydrogen absorbed by the metal comes from the dissolution of gaseous hydrogen (so that the solubility of hydrogen in the metal is proportional to the square root of the hydrogen partial pressure, following the Sieverts's law). Due to the resulting pressure decrease within these cracks, steam would be "sucked up" again. The hydrogen pickup would thus significantly increase. In theory, this process could be repeated until the hydrogen content in the metal is in equilibrium with the hydrogen partial pressure in the atmosphere.

There is no certainty that steam can access the pores/cracks at the metal-oxide interface (where the oxide is therefore delaminated from the metal). Indeed, in this case, the metallic side of pores at the metal-oxide interface would re-oxidize, which was not clearly evidenced. Furthermore, steam oxidation of the metallic surface may impede hydrogen pickup. Thus, it is possible that gaseous hydrogen is generated close to the pores at the metal-oxide interface and migrates through the oxide to join these pores. The oxidation of the metallic side of the cracks at the metal-oxide interface would take place in a later stage of the breakaway oxidation process. It would be associated with a decrease in hydrogen pickup fraction, which seems to occur a few hundreds of seconds after the breakaway oxidation transition (Fig. 8). Afterwards, there is possibly a second generation of pores/cracks at the metal-oxide interface.

It may seem surprising that more numerous pores and cracks parallel to the metal-oxide interface were observed in delayed oxidation regions (*i.e.* where the oxide is the thinner) than in the advanced oxidation regions. It can therefore be assumed that these pores and cracks were not interconnected and/or have formed during quenching rather than during oxidation. This suggests that the oxide was more brittle in delayed oxidation regions and/or that the accelerated transport of oxygen and hydrogen species to the metal via these pores and cracks would be counterbalanced by a decelerating effect of higher compressive stresses or particular characteristics of the oxide in these zones.

Oxide morphology appeared to be linked to undulation of the metal-oxide interface as well as oxide damage: oxide crystallites are shorter and wider with a larger density of micro-pores in the spalled sublayer and in delayed oxidation regions of the adherent sublayer of post-breakaway oxides than in pre-breakaway oxide layers or in the advanced oxidation regions of the adherent sublayer of post-breakaway oxides. These observations are consistent with those made in [40] for Zircaloy-4 oxidized at 1000°C, showing, on average, larger grains, better defined and less tortuous grain boundaries and more numerous micro-pores in post-breakaway oxide layers than in pre-breakaway oxide layers. With larger grains and flatter grain boundaries, the grain boundary surface area and therefore the interface energy are reduced and the overall energy is minimized. This change in grain morphology may result from the reduction of the stress level locally. It can be assumed that the transport of hydrogen and oxygen species is made easier in oxide layers with this morphology. In addition, pores are likely to coalesce and form cracks along grain boundaries. Larger and more equiaxed grains are expected to promote the formation of such cracks. Besides, there may be an accumulation of oxygen in delayed oxidation regions due for example, as discussed later, to a barrier effect of either domains where zirconia is monoclinic near the metal-oxide interface or pores when they are not connected. This would lead to further embrittlement of the oxide and making its cracking easier.

4.2. Stresses in the oxide layer

As shown in Section 3.5, the location of cracks within the oxide layer is related to the undulation of the metal-oxide interface. On the one hand, the cracks parallel to the metal-oxide interface within the oxide layer are preferentially located in the delayed oxidation regions, where metal-oxide delamination is also observed. On the other hand, radial cracks tend to form where the oxide is the thickest.

Internal stresses are generated within the oxide and the metallic substrate during oxidation [30]. They result from the strains associated with oxide layer growth, oxygen diffusion through the metal, β_{Zr} to $\alpha_{Zr}(O)$ phase transformation or phase transformation of zirconia, for example. These stresses are not yet well known to the authors' knowledge for oxidation temperatures as high as 1000°C. However, they are expected to be very different from those reported for oxidations carried out at lower temperatures, due to larger diffusion of oxygen into the metal, greater viscoplasticity of the metallic phases and pseudo-viscoplasticity of zirconia in particular [30]. The amplitude of internal stresses in the oxide layer is expected to decrease, at least on average, during oxidation [30].

The undulation of the metal-oxide interface probably results from minimization of strain energy. It is therefore likely to be associated, one the one hand, with stress levels lower in average than those expected for a metal-oxide interface without undulation, but also, one the other hand with more heterogeneous stress fields [42][43]. Compressive stresses in the oxide in the directions parallel to the oxide outer surface are expected to be the highest in the delayed oxidation regions, where radial stresses are positive while they are negative in the advanced oxidation regions. The locations where cracks and decohesion were observed are consistent with such stress fields, assuming that cracks form perpendicular to the maximum principal stress, as expected for brittle materials. Furthermore, higher compressive stresses may result in slower oxygen diffusion through the oxide [44] (due to a decrease in oxygen vacancy mobility [45]) and thus limit the oxidation rate. In that case, oxygen diffusion would be more difficult in the delayed oxidation regions, where the compressive stresses are expected to be the highest, and the undulation of the metal-oxide interface would be then accentuated.

The observations suggested that the undulation of the metal-oxide interface is connected to the size and the crystallographic orientation of $\alpha_{Zr}(O)$ grains and therefore to the crystallographic orientation of zirconia crystallites.

The undulations at the metal-oxide interface have a smaller amplitude and are closer one from another in the case of $M5_{Framatome}$ than in the case of Zircaloy-4, and the associated elongation of the metal-oxide interface is smaller. Thus, it may be assumed that the level and the heterogeneity of stresses generated near the metal-oxide interface during oxidation at 1000°C are smaller for $M5_{Framatome}$ than for Zircaloy-4.

4.3. Oxide phases and stoichiometry

The outer surface of the oxide layer formed at HT are black or dark grey before breakaway oxidation and exhibits a whitish/light grey appearance after breakaway oxidation. This colour change, which affects the outer surface of the oxide but not necessarily its bulk, is often associated with the oxide stoichiometry: sub-stoichiometric (by oxygen deficiency) zirconia formed at HT is generally black while stoichiometric zirconia tends to be more whitish [46]. Therefore, breakaway oxidation is associated with a change in oxide stoichiometry: pre-breakaway oxide may be sub-stoichiometric while post-breakaway oxide (or at least its outer surface) would be stoichiometric. The increase in stoichiometry may be related to heterogeneities in chemical composition, stress and/or oxidation rate, in particular close to the oxide-metal interface. The oxide stoichiometry (oxygen vacancies) may influence the diffusion of atoms through the oxide, the stability of the zirconia tetragonal phase or the oxide plasticity, or both.

At 1000°C, the oxide layer is constituted of a mixture of the monoclinic phase of zirconia (thermodynamically stable at this temperature) and the tetragonal phase (metastable at this temperature) [29]. Indeed, the tetragonal phase of zirconia can be stabilized at lower temperatures in the presence of anion vacancies [47] or some chemical or doping elements [48][49], compressive stresses [49][50] or small crystal size [48][51][52]. The volume fraction of the tetragonal phase of zirconia is generally greatest near the metal-oxide interface, where the oxide grains are the smallest [53][54] and the compressive stresses are the highest [50][55], and it diminishes during oxide growth [55]. The tetragonal phase of zirconia can be destabilized during oxidation [56] due to reduction of compressive stresses, increase of oxide grain size or recombination of defects in the oxide. The tetragonal to monoclinic phase transformation of zirconia is associated with strong lattice distortions and a significant volume expansion, which can locally generate additional stresses and induce a new phase transformation of zirconia, and the formation of pores (probably at grain boundaries) or even cracks within the oxide. The undulation of the metal oxide-interface and the heterogeneous distribution of pores and cracks in the oxide layers suggest that the tetragonal to monoclinic phase transformation of zirconia is heterogeneous near the metal oxide-interface.

The smaller oxide thickness at which breakaway oxidation occurs in the case of $M5_{Framatome}$ compared to Zircaloy-4 may be due to a higher initial fraction and a lower stability of the tetragonal phase of zirconia in the case of $M5_{Framatome}$, due to the effect of some alloying elements (tin and niobium in particular). Baek and Jeong [12] observed that the lower the tin content, the better the resistance to breakaway oxidation under steam at 1000°C. They proposed that the effect was related to the destabilization of the tetragonal phase in zirconia and to a faster cracking of the oxide layer in the presence of tin. The influence of these alloying elements on the stabilization of the tetragonal phase of zirconia probably does not rely on a direct effect but rather on the resulting oxygen vacancies concentration within the oxide [45].

4.4. Distribution of chemical elements in the oxide

A spatial redistribution of tin in Zircaloy-4 and niobium in $M5_{Framatome}$ was evidenced at the microscale in the oxide and the underlying metal after oxidation at 1000°C. Microchemical modulations in the oxide probably inherit from the metallic substrate which, at the same time as the oxide starts to form, transforms into the $\alpha_{Zr}(O)$ phase with a partition of some chemical elements (tin and niobium in particular) at the microscale. These microchemical heterogeneities may cause heterogeneities of structure and stoichiometry in the oxide layer formed on the microchemically heterogeneous prior-$\alpha_{Zr}(O)$ phase. It is likely that there is also segregation of tin and niobium in oxides formed at temperatures higher than 1000°C, at which no breakaway oxidation is observed, but in that case it can be assumed that chemical segregation does not have an effect on the structure of zirconia, remaining tetragonal.

The undulation of the metal-oxide interface appeared to be correlated to the microchemical modulations in its neighbourhood. Given the previous assumptions, this undulation could result from phase and stoichiometry heterogeneities in the oxide layer, themselves related to heterogeneities of chemical composition. Furthermore, the undulation of the metal-oxide interface may generate heterogeneous stresses and variations of oxygen diffusion through the oxide, which may enhance structure and stoichiometry heterogeneities in the oxide layer.

The mechanical properties of the oxide and the metallic substrate are likely to depend on the local chemical composition. For example, the results reported in [57] showed that an increase in niobium content reduced the creep rate of β_{Zr} at HT. Therefore, in the case of $M5_{Framatome}$, the mechanical properties of niobium enriched and oxygen depleted β_{Zr} layers (the partition of oxygen is the opposite of the distribution of niobium) and niobium depleted and oxygen enriched $\alpha_{Zr}(O)$ zones are probably not the same. This particular microstructure should have an effect on stresses and may contribute to the smaller undulations at the metal-oxide observed in the case of $M5_{Framatome}$ in comparison to Zircaloy-4, which shows a continuous $\alpha_{Zr}(O)$ layer without β_{Zr} phase platelets. The mechanical properties of zirconia depend on its stoichiometry and therefore on its (local) chemical composition. For example, sub-stoichiometric zirconia can show (pseudo-)superplastic properties at HT [58].

4.5. Suggested mechanism for breakaway oxidation

Breakaway oxidation around 1000°C is probably the consequence of a relatively complex coupling between several physicochemical and mechanical phenomena. Fig. 24 schematizes the relationships that may exist between the parameters and the properties that may influence the occurrence of breakaway oxidation. Several factors are more or less directly linked to stresses, either as a source (*e.g.* gradient of vacancies within the oxide, epitaxy between zirconium and zirconia, phase transformation) or as a consequence (*e.g.* stability of zirconia tetragonal phase, transport of oxygen through the oxide, oxide cracking).

On the basis of the results and the assumptions that have been previously presented, the following mechanism of breakaway oxidation around 1000°C is proposed:

- Oxide layer formation and partition of chemical elements: water is dissociated at the material outer surface, oxygen diffuses through the metal leading to the formation of both $\alpha_{Zr}(O)$ and sub-stoichiometric, principally tetragonal (structure stabilized because of large stresses, sub-stoichiometry and small grains), zirconia, with partition of some chemical elements over a few microns.
- Growth of a two-phase (tetragonal and monoclinic zirconia) sub-stoichiometric oxide: oxygen anions diffuse from the outer surface to the metal-oxide interface where the

chemical reaction takes place, leading to oxide growth. Columnar crystallites grow perpendicular to the metal-oxide interface and their size increases in the course of oxidation, due to a decrease of stresses in particular. Compressive stress levels and density of vacancies are larger in the vicinity of the metal-oxide interface than at the outer surface. Thus, from a certain thickness, the oxide layer may be mainly constituted of monoclinic zirconia in its outer part and of tetragonal zirconia near the metal-oxide interface, at least since tetragonal zirconia has not been destabilized by any factor.

- Heterogeneous phase transformation of zirconia: the crystallographic orientation of zirconia crystals is linked to that of the underlying $\alpha_{Zr}(O)$ crystals and to the stresses generated during oxidation. In addition, the oxide inherits from the microchemical heterogeneities of the metallic substrate. Thus, the oxide is constituted of micro-zones with different chemical compositions, structures, densities of vacancies, stoichiometries and mechanical properties. These heterogeneities together with those of the metallic substrate lead to heterogeneity of the stress field in the oxide. In zones where stresses are the lowest, the oxide crystallites are the coarsest and the density of vacancy is the lowest (zones depleted in tin for example), tetragonal zirconia transforms into monoclinic zirconia. This martensitic transformation progresses heterogeneously and the strains that result from it, together with the formation of pores by recombination of vacancies (mainly near the metal-oxide interface, at grain boundaries and/or at the boundary between zones where zirconia is monoclinic and tetragonal, monoclinic zirconia tending to be less sub-stoichiometric than tetragonal zirconia), generate stress concentrations. The formation of pores can be promoted by these stresses.
- Heterogeneous oxide growth and local saturation in oxygen: oxide growth is slower where zirconia is monoclinic (due to the lower diffusivity of oxygen through it) and pores that are not interconnected are numerous (barrier effect against oxygen transport). Furthermore, it can be assumed that the local oxidation rate depends on the local chemical composition and the crystallographic orientation. The metal-oxide interface thus appears undulated. Where the oxide layer is the thinnest, the oxide tends to be saturated in oxygen so that it is closer to stoichiometry and more brittle than where the oxide is thicker. On the one hand, the undulation of the metal-oxide interface leads to a reduction of average stresses along hoop and axial directions. On the other hand, it causes radial stresses and is an additional source of mechanical heterogeneities.
- Local micro-cracking and decohesion of the metal-oxide interface: micro-cracks parallel to the metal-oxide interface and decohesion of the oxide and the metallic substrate initiate at pores, primarily where oxide growth is retarded. Indeed, at this location, zirconia tends to be monoclinic, stoichiometric, more brittle and porous, and it is loaded in tension along the radial direction. This damage of the oxide and the metal-oxide interface induces relaxation and redistribution of stresses in the oxide.
- Oxide cracking, acceleration of oxygen and hydrogen transport and absorption of hydrogen: under the effect of stress relaxation, grains become coarser where oxide growth is retarded. Zirconia mainly tetragonal in front of zones where the oxide is the thickest is susceptible to transform into monoclinic zirconia. Stresses in these regions become positive along hoop and axial directions. Radial cracks propagate in the zones and interact with cracks parallel of the metal-oxide interface, preferentially located where the oxide layer is the thinnest.
- Steam can then reach more or less directly the vicinity of the metal-oxide interface via cracks, acting as short-circuit transport paths. Because of the faster transport of oxygen through the oxide, the oxidation rate increases in average. Due to microchemical partitioning and to stress and oxidation rate heterogeneity, in particular close to the metal-oxide interface and to pores and cracks, the oxide is progressively saturated in

oxygen (filling of vacancies) and becomes stoichiometric. It then appears whitish. As a result of oxidation, the partial pressure of gaseous hydrogen near the metal-oxide interface increases and hydrogen is absorbed by the metal. The pressure within the cracks then decreases so that hydrogen can enter through them again. This self-sustaining process leads to a continuous hydrogen pickup.

- A fresh oxide sublayer may start to grow more or less directly after oxide cracking and decohesion of the metal-oxide interface. The oxidation rate is faster where the existing oxide sublayer is the thinnest. At these locations, there are a lot of cracks parallel to the metal-oxide interface and the oxide crystallites are wider, better organized and have lost their adherence to the metal, so that the transport of oxygen and hydrogen species though the oxide and their access to the metal-oxide interface are made easier. Under these conditions, the undulation of the metal-oxide interface first diminishes then becomes the opposite of the undulation of the interface with the prior oxide sublayer: oxidation is enhanced at locations where the oxidation was earlier delayed. The new oxide sublayer rapidly losses the protectiveness it had when it started to grow, under the effects of the previously discussed phenomena (*e.g.* destabilization of tetragonal zirconia, formation then coalescence of pores and cracks in the oxide).
- Finally, the global oxidation and hydrogen pickup kinetics appear to be nearly linear.

This mechanism is rather consistent with the one postulated by Leistikow and Schanz in the early 1980's [9][10]. It is supported by additional experimental evidences and provides new insights into the potential effects of microchemical heterogeneities in particular.

5. Conclusions

The breakaway oxidation of low tin Zircaloy-4 and $M5_{Framatome}$ alloys when oxidized under flowing steam (at atmospheric pressure) has been studied.

Oxidation tests performed at various temperatures between 950 and 1050°C with holding times between 55 and 15000 s have shown that the oxidation of $M5_{Framatome}$ before breakaway oxidation was slower than that of Zircaloy-4. According to visual examination and to weight gain and hydrogen content measurements, breakaway oxidation of Zircaloy-4 occurred for oxidation times shorter than 15000 s at 950, 975, 1000 and 1025°C. The incubation time needed for breakaway oxidation was the lowest at 1000°C and increased when deviating from this temperature: it was about 9500-15000 s at 950°C, 5000-7500 s at 975°C, 5000-5500 s at 1000°C and 9500-15000 s at 1025°C. The higher the temperature within this range the larger the weight gain at which breakaway oxidation of Zircaloy-4 occurred: it was around 8-11 mg/cm^2 at 950 and 975°C, 13-14 mg/cm^2 at 1000°C and 25-34 mg/cm^2 at 1025°C. No breakaway oxidation was evidenced at 1050°C. The results about breakaway oxidation of Zircaloy-4 at 1000°C were similar whether the cladding sample was oxidized on both its outer and inner surface or on its outer surface only.

$M5_{Framatome}$ (from the most recent batch tested) two-sided oxidized did not show breakaway oxidation at 950, 975, 1025 and 1050°C for times up to 15000 s. It has nonetheless been suggested that breakaway oxidation occurred after approximately 15000 s at 1025°C, for a weight gain of 15 mg/cm^2. The resistance to breakaway oxidation of $M5_{Framatome}$ at 1000°C was even higher for the most recent material batches than for the one tested in the early 2000's.

Furthermore, the results about the breakaway oxidation of $M5_{Framatome}$ depended on the oxidation type. For the former batch, breakaway oxidation was observed after 15000 s, for a weight gain of about 12 mg/cm^2, in the case of two-side oxidation and after about 5000-5500 s, for a weight gain of about 8-9 mg/cm^2, in the case of one-side oxidization. The newest batch

did not show any sign of breakaway oxidation for times up to 15000 s in the case of two-side oxidization while it exhibited breakaway oxidation after approximately 9500 s at 1000°C, for a weight gain close to 11-12 mg/cm^2, in the case of one-side oxidation.

One-side oxidation tests associated with post-test hydrogen content measurements were performed in steam at 1000°C on M5$_{Framatome}$ samples with various contents of Nb (0.87 and 1.25 wt%), Fe (195 and 715 wppm), O (500, 930 and 1680 wppm), S (14 and 41 wppm) and Hf (62 and 487 wppm). The results showed that the pre-breakaway oxidation kinetics and the incubation time needed for breakaway oxidation were not significantly modified by the chemical composition variations investigated. After the onset of breakaway oxidation, weight gains and hydrogen uptake data were scattered.

It was shown for both alloys that the fraction of hydrogen absorbed by the material was very high (at least 50%) at the onset of breakaway oxidation and then decreased to a few tens of percent for longer oxidation times. Microstructural observations were performed on Zircaloy-4 and M5$_{Framatome}$ samples (batches from the early 2000's) one-sided oxidized at 1000°C. Breakaway oxidation occurred for an average oxide thickness of approximately 50 µm for Zircaloy-4 and 25 µm for M5$_{Framatome}$, but for comparable oxidation times, the oxidation kinetics of M5$_{Framatome}$ being slower. After quenching, post-breakaway oxide layers showed locally more numerous cracks and micro-pores, and shorter and wider crystallites, than pre-breakaway oxide layers. Post-breakaway oxide layers spalled partially or completely during quenching. The metal-oxide interface appeared undulated (undulation amplitude of a few microns) after 15-20 min oxidation at 1000°C, *i.e.* well before breakaway oxidation, for an average oxide thickness of approximately 30 µm for Zircaloy-4 and 15 µm for M5$_{Framatome}$. The micro-scale undulations at the metal-oxide interface were, in average, of lower amplitude, closer one from another, less variable and more homogeneously distributed in the case of M5$_{Framatome}$ than in the case of Zircaloy-4. Chemical microanalysis revealed microscale segregation of tin in Zircaloy-4 and of niobium in M5$_{Framatome}$ during oxidation at 1000°C, with a certain continuity of the chemical modulations on either side of the metal-oxide interface. The undulation of the metal oxide-interface seemed to be correlated to the distribution of tin and niobium within the oxide and the metallic substrate.

On the basis of the results obtained, a mechanism of breakaway oxidation around 1000°C has been postulated. According to this mechanism, the local destabilization of tetragonal phase of zirconia would be the initiator. This phase transformation would be heterogeneous due to microchemical partitions and/or to crystallographic heterogeneities in both the metal and the oxide. The succession of events (heterogeneous oxide growth, local saturation in oxygen, local oxide micro-cracking, decohesion of the metal-oxide interface, oxide cracking) that would result from this phase transformation would lead to breakaway oxidation. Nevertheless, further work must be done to verify some of the assumptions, in order to explain the differences between materials in particular.

6. Acknowledgements

We thank M. Abdelhak, P. Bonnaillie, P. Bossis, C. Cobac, D. Gilbon, D. Hamon, C. Hossepied, F. Michel, S. Paradowski, E. Rouesne, S. Urvoy, J.P. Mardon, EDF and Framatome for their contributions to this work. This work was funded by the French Nuclear Institute in the framework of the GAINES project.

Data Availability

The raw/processed data required to reproduce these findings cannot be shared at this time due to technical or time limitations.

References

[1] L. Baker, L.C. Just, Studies of Metal-Water Reactions at High Temperatures. III. Experimental and Theoretical Studies of the Zirconium-Water Reaction, ANL-6548, Argonne National Laboratory, Lemont, IL, 1962.

[2] J.V. Cathcart, R.E. Pawel, R.A. McKee, R.E. Druschel, G.J. Yurek, J.J. Campbell, S.H. Jury, Zirconium Metal-Water Oxidation Kinetics IV. Reaction Rate Studies, ORNL/NUREG-17, US Nuclear Regulatory Commission, Washington, D.C, 1977.

[3] F. Nagase, T. Otomo, H. Uetsuka, Oxidation Kinetics of Low-Sn Zircaloy-4 at the Temperature Range from 773 to 1573K, Journal of Nuclear Science and Technology 40 (2003) 213-219.

[4] J.H. Baek, K.B. Park, Y.H. Jeong, Oxidation kinetics of Zircaloy-4 and Zr-1Nb-1Sn-0.1Fe at temperatures of 700-1200°C, Journal of Nuclear Materials 335 (2004) 443-456.

[5] L. Portier, T. Bredel, J.C. Brachet, V. Maillot, J.P. Mardon, A. Lesbros, Influence of Long Service Exposures on the Thermal-Mechanical Behaviour of Zy-4 and M5™ Alloys in LOCA Conditions, Journal of ASTM International 2 (2005) JAI12468.

[6] M. Le Saux, V. Vandenberghe, P. Crébier, J.C. Brachet, D. Gilbon, J.P. Mardon, B. Sebbari, Influence of Steam Pressure on the High Temperature Oxidation and Post-Cooling Mechanical Properties of Zircaloy-4 and M5™ Cladding (LOCA Conditions), Zirconium in the Nuclear Industry: 17th Volume, STP1543, B. Comstock and P. Barbéris, Eds., ASTM International, West Conshohocken, PA, 2014, pp. 1002-1053.

[7] J.C. Brachet, V. Vandenberghe, Comments to papers of J. H. Kim et al. [1] and M. Große et al. [2] recently published in JNM "On the hydrogen uptake of Zircaloy-4 and M5™ alloys subjected to steam oxidation in the 1100-1250°C temperature range", Journal of Nuclear Materials 395 (2009) 169-172.

[8] M. Große, M. Steinbrueck, B. Shillinger, A. Kaestner, In-situ Investigations of the Hydrogen Uptake of Zirconium Alloys during Steam Oxidation, Zirconium in the Nuclear Industry: 18th International Symposium, ASTM STP 1597, R. Comstock and A. Motta, Eds., ASTM International, West Conshohocken, PA, 2018, 1114-1135.

[9] S. Leistikow, G. Schanz, Oxidation Kinetics and Related Phenomena of Zircaloy-4 Fuel Cladding Exposed to High Temperature Steam and Hydrogen-Steam Mixtures under PWR Accident Conditions, Nuclear Engineering and Design 103 (1987) 65-84.

[10] S. Leistikow, G. Schanz, H.V. Berg, A.E. Aly, Comprehensive presentation of extended Zircaloy-4 steam oxidation results (600-1600°C), OECD-NEA-CSNI/IAEA Specialists Meeting on Water Reactor Fuel Safety and Fission Product Release in Off-Normal and Accident Conditions, Risö National Laboratory, Denmark, 1983.

[11] M. Billone, Y. Yan, T. Burtseva, R. Daum, Cladding Embrittlement during Postulated Loss-of-Coolant Accidents, NUREG/CR-6967, Argonne National Laboratory, Lemont, IL, 2008.

[12] J.H. Baek, Y.H. Jeong, Breakaway phenomenon of Zr-based alloys during a high-temperature oxidation, Journal of Nuclear Materials 372 (2008) 152-159.

[13] J.A. Gresham, Updated Westinghouse Breakaway Oxidation Testing/Behavior (Non-Proprietary), Westinghouse letter report to NRC LTR-NRC-08-29, US NRC ADAMS Accession No. ML081700587, 2008.

[14] Z. Hózer, C. Gyori, L. Matus, M. Horváth,, Ductile-to-brittle transition of oxidised Zircaloy-4 and E110 claddings, Journal of Nuclear Materials 373 (2008) 415-423.

[15] D.J. Park, J.Y. Park, Y.H. Jeong, J.Y. Lee, Microstructural characterization of ZrO_2 layers formed during the transition to breakaway oxidation, Journal of Nuclear Materials 399 (2010) 208-211.

[16] H.H. Kim, J.H. Kim, J.Y. Moon, H.S. Lee, J.J. Kim, Y.C. Chai, Y.C., High-temperature Oxidation Behavior of Zircaloy-4 and Zirlo in Steam Ambient, Journal of Materials Science & Technology 26 (2010) 827-832.

[17] M. Große, Comparison of the high temperature steam oxidation kinetics of advanced cladding materials, Nuclear Technology 170 (2010) 272-279.

[18] M. Steinbrück, J. Birchley, A.V. Boldyrev, A.V. Goryachev, M. Große, T.J. Haste, Z. Hózer, A.E. Kisselev, V.I. Nalivaev, V.P. Semishkin, L. Sepold, J. Stuckert, N. Vér, M.S. Veshchunov, High-temperature oxidation and quench behaviour of Zircaloy-4 and E110 cladding alloys, Progress in Nuclear Energy 52 (2010) 19-36.

[19] H.K. Yueh, R.J. Comstock, B. Dunn, M. Le Saux, Y.P. Lin, D. Lutz, D.J. Park, E. Perez-Fero, Y. Yan, Loss of Coolant Accident Testing Round Robin, TopFuel 2013, Charlotte, NC, September 15–19, 2013, American Nuclear Society, La Grange Park, IL, USA.

[20] J. Desquines, D. Drouan, S. Guilbert, P. Lacote, Embrittlement of Pre-Hydrided Zircaloy-4 by Steam Oxidation under Simulated LOCA Transients, Journal of Nuclear Materials 469 (2016) 20-31.

[21] I. Turque, R. Chosson, M. Le Saux, J.C. Brachet, V. Vandenberghe, J. Crépin, A.F. Gourgues-Lorenzon, Mechanical Behavior at High Temperatures of Highly Oxygen- or Hydrogen-Enriched α and Prior-β Phases of Zirconium Alloys, Zirconium in the Nuclear Industry: 18th International Symposium, ASTM STP1597, R. J. Comstock and A. T. Motta, Eds., ASTM International, West Conshohocken, PA, 2018, pp. 240-280.

[22] J.C. Brachet, D. Hamon, M. Le Saux, V. Vandenberghe, C. Tofflon-Masclet, E. Rouesne, S. Urvoy, J.L. Béchade, C. Raepsaet, J.L. Lacour, G. Bayon, F. Ott, Study of secondary hydriding at high temperature in zirconium based nuclear fuel cladding tubes by coupling information from neutron radiography/tomography, electron probe micro analysis, micro elastic recoil detection analysis and laser induced breakdown spectroscopy microprobe, Journal of Nuclear Materials 488 (2017) 267-286.
[23] M. Le Saux, J.C. Brachet, V. Vandenberghe, E. Rouesne, S. Urvoy, A. Ambard, R. Chosson, Effect of a pre-oxide on the high temperature steam oxidation of Zircaloy-4 and $M5_{Framatome}$ alloys, Journal of Nuclear Materials 518 (2019) 386-399.
[24] Y. Yan, T. Burtseva, M. Billone, High-Temperature Steam-Oxidation Behavior of Zr-1Nb Cladding Alloy E110, Journal of Nuclear Materials 393 (2009) 433-448.
[25] M. Steinbrück, N. Vér, M. Große, Oxidation of Advanced Zirconium Cladding Alloys in Steam at Temperatures in the Range of 600-1200°C, Oxidation of Metals 76 (2011) 215-232.
[26] M. Steinbrück, Prototypical experiments relating to air oxidation of Zircaloy-4 at high temperatures, Journal of Nuclear Materials 392 (2009) 531-544.
[27] J.C. Brachet, V. Vandenberghe-Maillot, L. Portier, D. Gilbon, A. Lesbros, N. Waeckel, J.P. Mardon, Hydrogen Content, Preoxidation, and Cooling Scenario Effects on Post-Quench Microstructure and Mechanical Properties of Zircaloy-4 and M5™ Alloys in LOCA Conditions, Journal of ASTM International 5 (2008).
[28] S. Kawasaki, T. Furuta, M. Suzuki, Oxidation of Zircaloy-4 under High Temperature Steam Atmosphere and Its Effect on Ductility of Cladding, Journal of Nuclear Science and Technology 15 (1979) 589-596.
[29] D. Gosset, M. Le Saux, In-situ X-ray diffraction analysis of zirconia layer formed on zirconium alloys oxidized at high temperature, Journal of Nuclear Materials 458 (2015) 245-252.
[30] M. Le Saux, T. Guilbert, J.C. Brachet, An approach to study oxidation-induced stresses in Zr alloys oxidized at high temperature, Corrosion Science 140 (2018) 79-91.
[31] J. Godlewski., How the Tetragonal Zirconia is Stabilized in the Oxide Scale that is Formed on a Zirconium Alloy Corroded at 400°C in Steam, Zirconium in the Nuclear Industry: Tenth International Symposium, ASTM STP 1245, A.M. Garde and E.R. Bradley, Eds, American Society for Testing and Materials, Philadelphia, 1994, pp. 663-684.
[32] A. Couet, A.T. Motta, R.J. Comstock, Hydrogen pickup measurements in zirconium alloys: Relation to oxidation kinetics, Journal of Nuclear Materials 451 (2014) 1-13.
[33] B. Cox, Oxidation of Zirconium and its Alloys, Advances in Corrosion Science and Technology, M. Fontana and R. W. Staehle, Eds., Plenum Press, New York, 1976.
[34] J.C. Brachet, C. Toffolon-Masclet, D. Hamon, T. Guilbert, G. Trego, J. Jourdan, A. Stern, C. Raepsaet, Oxygen, Hydrogen and Main Alloying Chemical Elements Partitioning Upon Alpha-Beta Phase Transformation in Zirconium Alloys, Solid State Phenomena 172-174 (2011) 753-759.
[35] Diffusion in Solid Metals and Alloys, H. Mehrer (Ed), Landolt-Börnstein: Numerical Data and Functional Relationships in Science and Technology - New Series. Group III: Crystal and Solid State Physics, Volume 26.
[36] X. Ma, C. Toffolon-Masclet, T. Guilbert, D. Hamon, J.C. Brachet, Oxidation kinetics and oxygen diffusion in low-tin Zircaloy-4 up to 1523 K, Journal of Nuclear Materials 377 (2008) 359-369.
[37] G.J. Yurek, J.V. Cathcart, R.E. Pawel, Microstructures of the scales formed on zircaloy-4 in steam at elevated temperatures. Oxidation of Metals 10 (1976) 255-276.
[38] M. Große, R. Simon, Analysis of Tin Diffusion in Zircaloy-4 and Tin Redistribution after Steam Oxidation by Means of X-ray Fluorescence Measurements, Advanced Engineering Materials 11 (2009) 483-487.
[39] M. Große, E. Lehmann, M. Steinbrück, G. Kühne, J. Stuckert, Influence of oxide layer morphology on hydrogen concentration in tin and niobium containing zirconium alloys after high temperature steam oxidation, Journal of Nuclear Materials 385 (2009) 339-345.
[40] D.J. Park, J.Y. Park, Y.H. Jeong, J.Y. Lee, Microstructural characterization of ZrO_2 layers formed during the transition to breakaway oxidation, Journal of Nuclear Materials 399 (2010) 208-211.
[41] J.C. Brachet, J. Pelchat, D. Hamon, R. Maury, P. Jacques, J.P., Mardon, Mechanical behavior at Room Temperature and Metallurgical study of Low-Tin Zy-4 and M5™ (Zr-NbO) alloys after oxidation at 1100°C and quenching. Technical Committee Meeting on Fuel Behaviour under Transient and LOCA Conditions, IAEA-TECDOC-1320, Halden, Norway, 2001, pp. 139-158.
[42] M. Parise, O. Sicardy, G. Cailletaud, Modelling of the mechanical behavior of the metaloxide system during Zr alloy oxidation, Journal of Nuclear Materials 256 (1998) 35-46.
[43] V. Optasanu, L. Raceanu, T. Montesin, Simulation of Metal/Oxide Interface Mobility: Effects of Mechanical Stresses on Geometrical Singularities, Defect and Diffusion Forum 323-325 (2012) 109-114.
[44] G. Zumpicchiat, S. Pascal, M. Tupin, C. Berdin-Méric, Finite element modelling of the oxidation kinetics of Zircaloy-4 with a controlled metal-oxide interface and the influence of growth stress, Corrosion Science 100 (2015) 209-221.
[45] K. Sato, K. Suzuki, R. Narumi, K. Yashiro, T. Hashida, J. Mizusaki, Ionic Conductivity in Uniaxial Micro Strain/Stress Fields of Yttria-Stabilized Zirconia, Japanese Journal of Applied Physics 50 (2011) 055803.

[46] E.S. Sarkisov, N.T. Chebotarev, A.A. Nevzorova and A.I. Zver'kov, Oxidation of zirconium at high temperature and structure of the primary oxide film, Atomic Energy 5 (1958) 1465-1470.
[47] X. Lu, K. Liang, S. Gu, Y. Zheng, H. Fang, Effect of Oxygen Vacancies on Transformation of Zirconia at Low Temperatures, Journal of Materials Science 32 (1997) 6653-6656.
[48] P. Barberis, Zirconia Powders and Zircaloy Oxide Films: Tetragonal Phase Evolution during 400°C Autoclave Tests, Journal of Nuclear Materials 226 (1995) 34-43.
[49] H. Beie, A. Mitwalsky, F. Garzarolli, H. Ruhmann, H. Sell, Examinations of the Corrosion Mechanism of Zirconium Alloys, Proceedings of the 10th International Symposium on Zirconium in the Nuclear Industry, ASTM STP 1245, ASTM International, West Conshohocken, PA, 1994.
[50] J. Godlewski, J. Gros, M. Lambertin, J. Wadier, H. Weidinger, Raman Spectroscopy Study of the Tetragonal-to-monoclinic Transition in Zirconium Oxide Scales and Determination of Overall Oxygen Diffusion by Nuclear Microanalysis of O^{18}, Proceedings of the 9th International Symposium on Zirconium in the Nuclear Industry, ASTM STP 1132, ASTM International, West Conshohocken, PA, 1991, 25520S.
[51] D. Simeone, G. Baldinozzi, D. Gosset, S. Le Caër, Phase Transition of Pure Zirconia under Irradiation: A Textbook Example, Nuclear Instruments and Methods in Physics Research Section B: Beam Interactions with Materials and Atoms B 250 (2006) 95-100.
[52] R.C. Garvie, Thermodynamics of the tetragonal to monoclinic phase transformation in constrained zirconia microcrystals – Part 2 in the presence of an applied stress field, Journal of Materials Science 20 (1985) 3479-3486.
[53] J.Y. Park, H.G. Kim, Y.H. Jeong, Y. H. Jung, Crystal Structure and Grain Size of Zr Oxide Characterized by Synchrotron Radiation Microdiffraction, Journal of Nuclear Materials 335 (2004) 433-442.
[54] A. Yilmazbayhan, E. Breval, A.T. Motta, R.J. Comstock, Transmission Electron Microscopy Examination of Oxide Layers Formed on Zr Alloys, Journal of Nuclear Materials 349 (2006) 265-281.
[55] N. Pétigny, P. Barberis, C. Lemaignan, C. Valot, M. Lallemant, In Situ XRD Analysis of the Oxide Layers Formed by Oxidation at 743 K on Zircaloy 4 and Zr-1NbO, Journal of Nuclear Materials 280 (2000) 318-330.
[56] R. Guillou, M. Le Saux, E. Rouesne, D. Hamon, C. Toffolon-Masclet, D. Menut, J.C. Brachet, J.L. Béchade, D.Thiaudière, In-situ time-resolved study of structural evolutions in a zirconium alloy during high temperature oxidation and cooling, Materials Characterization 158 (2019) 109971.
[57] G. Trego, Comportement en Fluage à Haute Température dans le Domaine Biphasé ($\alpha + \beta$) du M5, Ph.D. thesis, Ecole des Mines de Paris, France, 2012.
[58] Y. Maehara, T.G. Langdon, Review Superplasticity in Ceramics, Journal of Materials Science 5 (1990) 2275-2286.

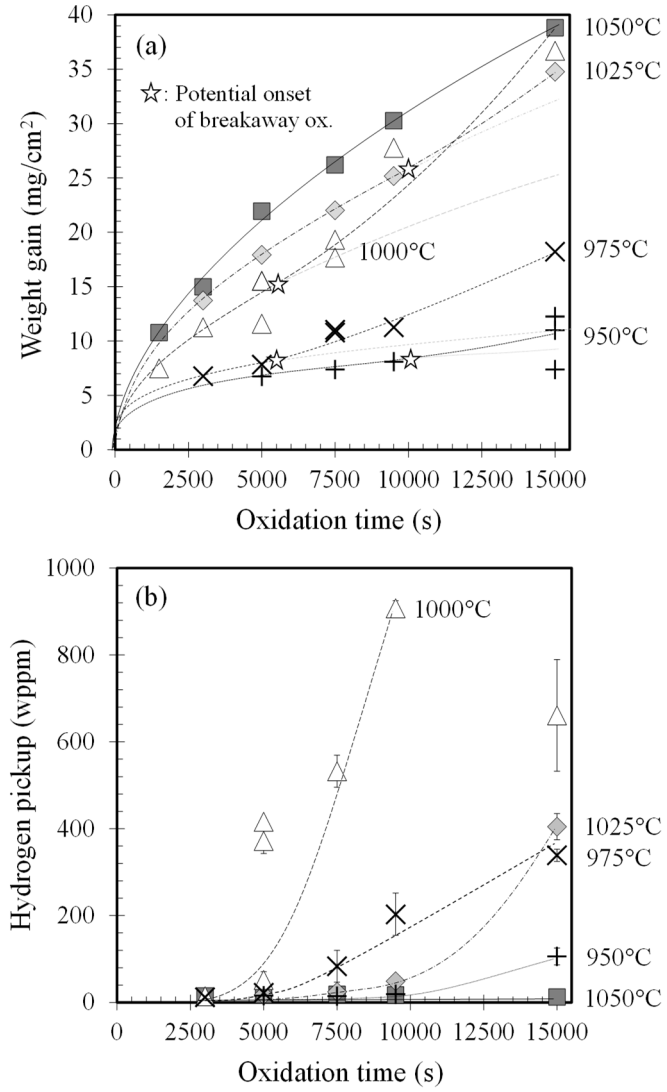

Fig. 1. Evolution of (a) the weight gain (the trend lines follow power laws up to the stars, indicating potential onset of breakaway oxidation, after which the trends deviate from the original power law fits) and (b) the hydrogen pickup (reduced to the cladding outer surface; error bars represent the standard deviation on the hydrogen contents measured for each sample) as a function of the oxidation time under steam at 950, 975, 1000, 1025 and 1050°C (two-side oxidation) for Zircaloy-4 (batch 2).

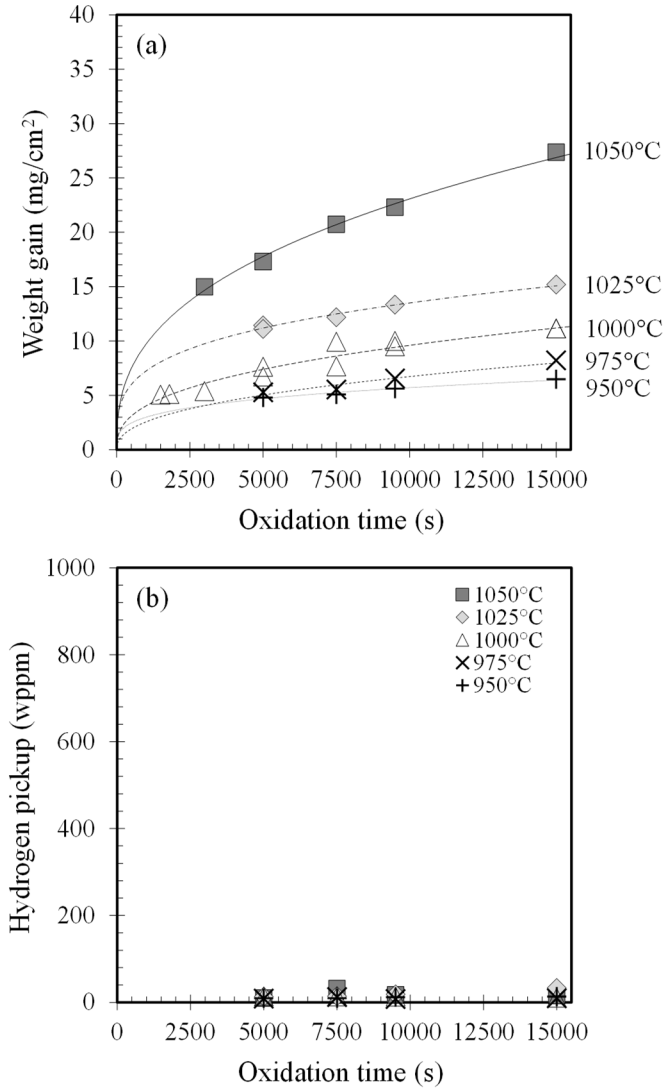

Fig. 2. Evolution of (a) the weight gain (the trend lines follow power laws) and (b) the hydrogen pickup (reduced to the cladding outer surface) as a function of the oxidation time under steam at 950, 975, 1000, 1025 and 1050°C (two-side oxidation) for $M5_{Framatome}$ (batch 2).

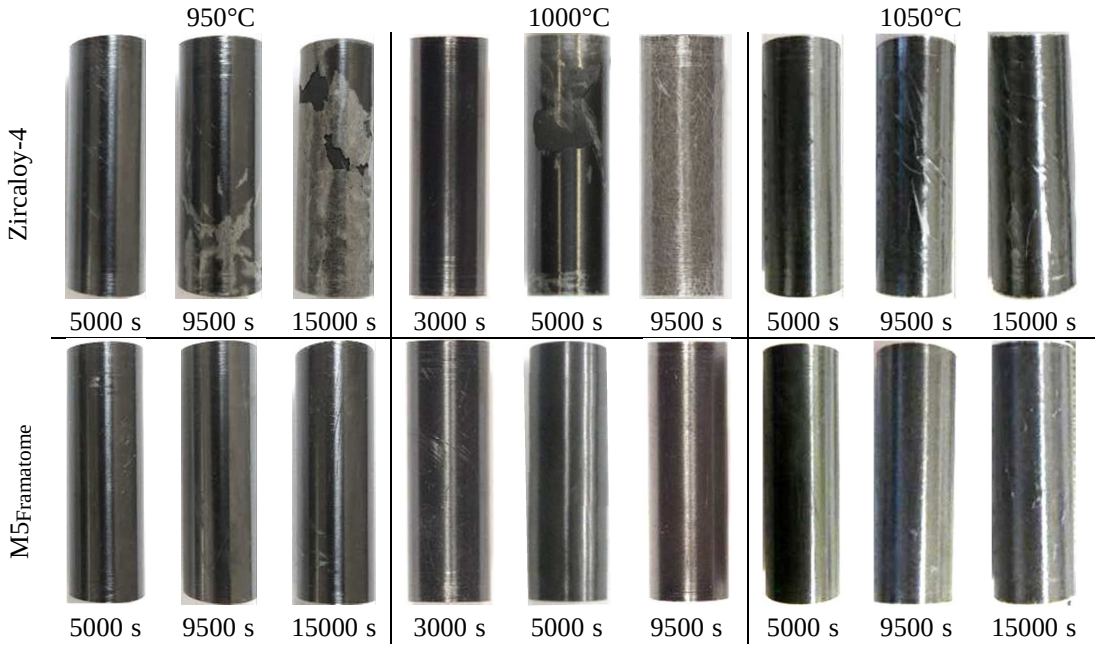

Fig. 3. Post-quenching appearance of Zircaloy-4 (batch 2) and $M5_{Framatome}$ (batch 2) cladding specimens two-sided oxidized in steam at 950, 1000 and 1050°C.

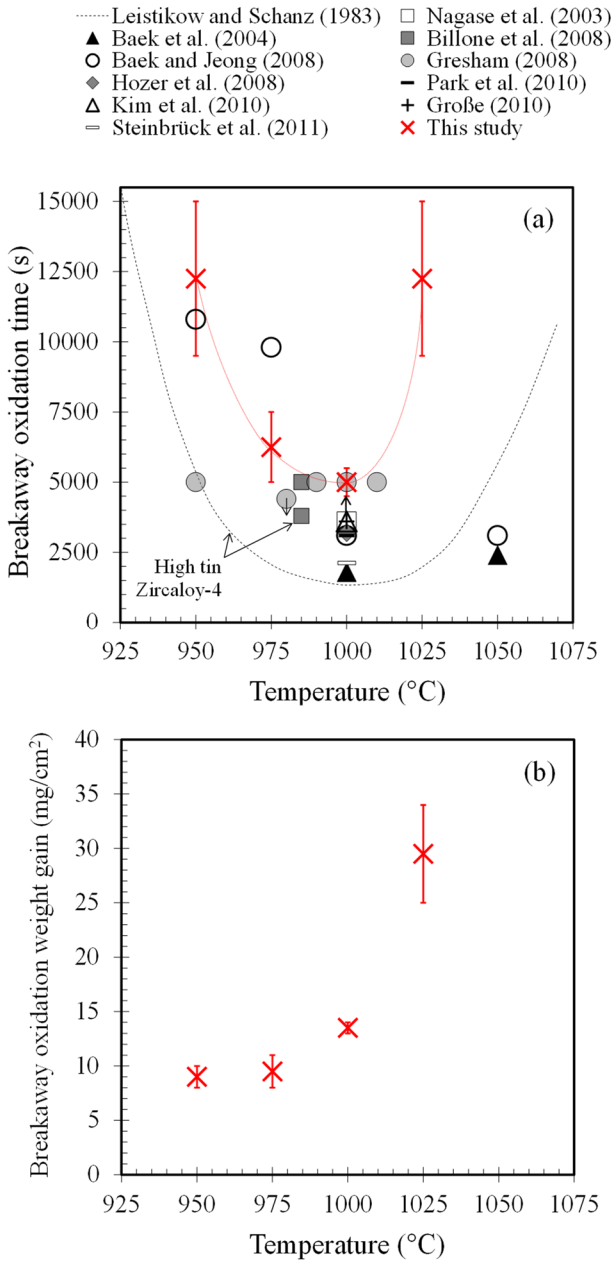

Fig. 4. Evolution of the incubation (a) time and (b) weight gain needed for breakaway oxidation of Zircaloy-4 as a function of temperature; comparison to data reported by Leistikow and Schanz [9], Nagase *et al.* [3], Billone *et al.* [11], Baek et Jeong [12], Gresham [13], Hozer *et al.* [14], Park *et al.* [15], Kim *et al.* [16], Große [17] and Steinbrück *et al.* [18].

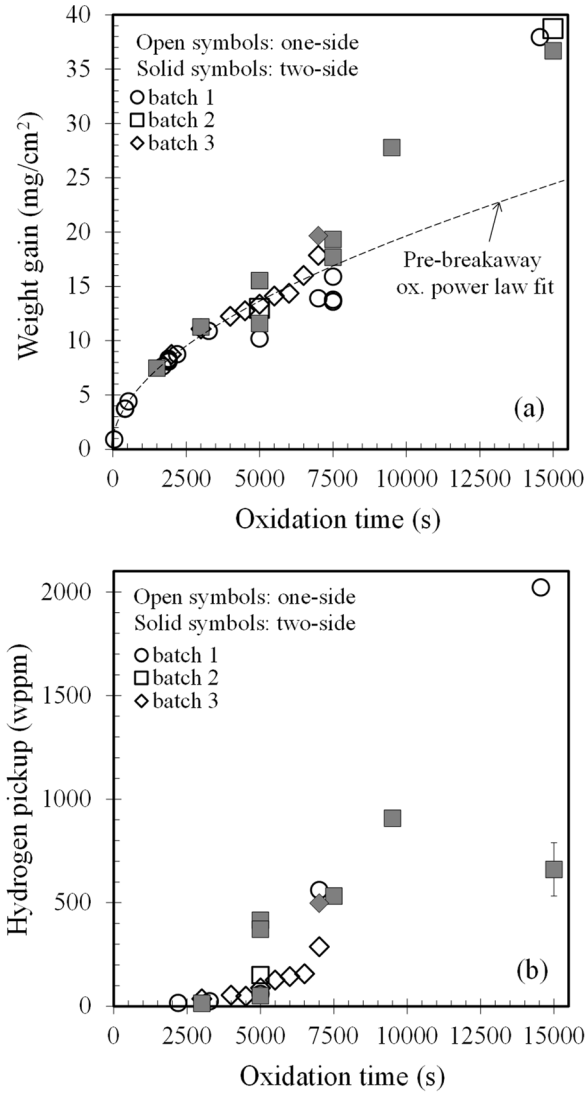

Fig. 5. Evolution of (a) the weight gain and (b) the hydrogen pickup (reduced to the cladding outer surface) as a function of the oxidation time for various batches of Zircaloy-4 one-sided or two-sided oxidized under steam at 1000°C.

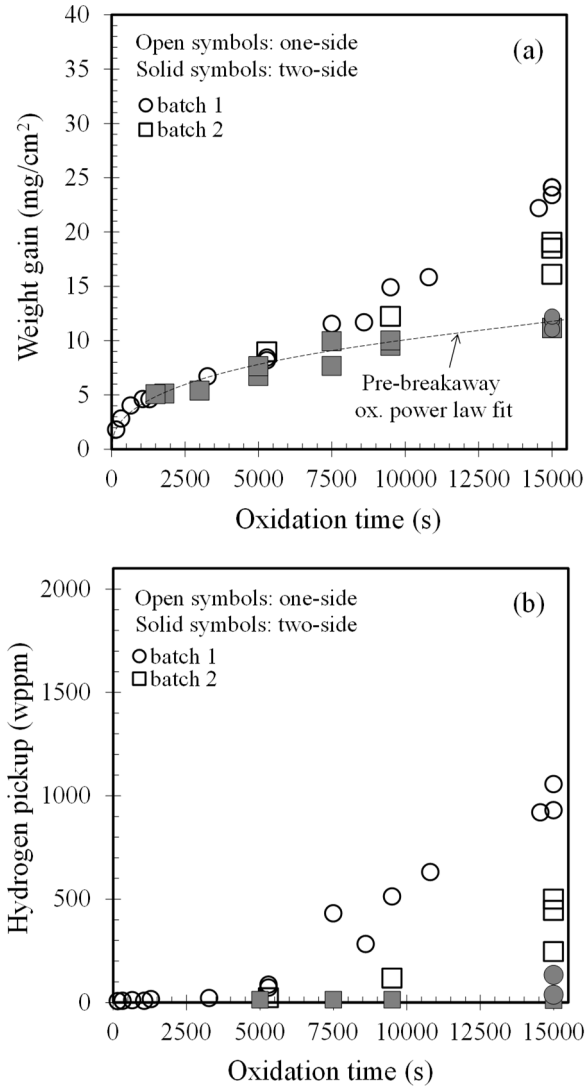

Fig. 6. Evolution of (a) the weight gain and (b) the hydrogen pickup (reduced to the cladding outer surface) as a function of the oxidation time for various batches of $M5_{Framatome}$ one-sided or two-sided oxidized under steam at 1000°C.

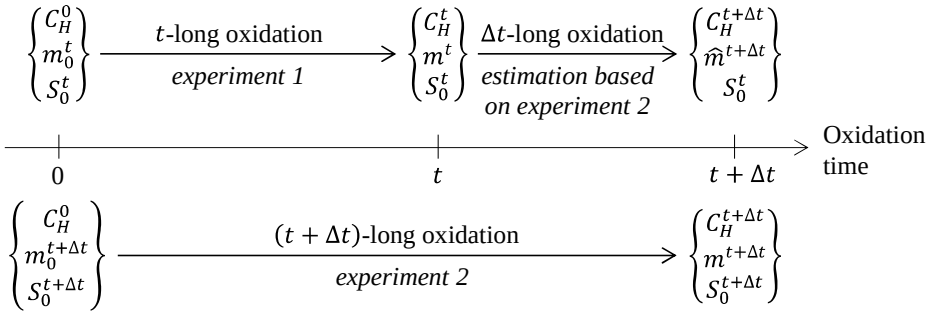

Fig. 7. Parameters used in Eqs. (1) and (2) to calculate the "instantaneous" hydrogen pickup fraction over a time period $[\boldsymbol{t}; \boldsymbol{t + \Delta t}]$ from the data of two experiments performed on samples with different initial mass and surface area.

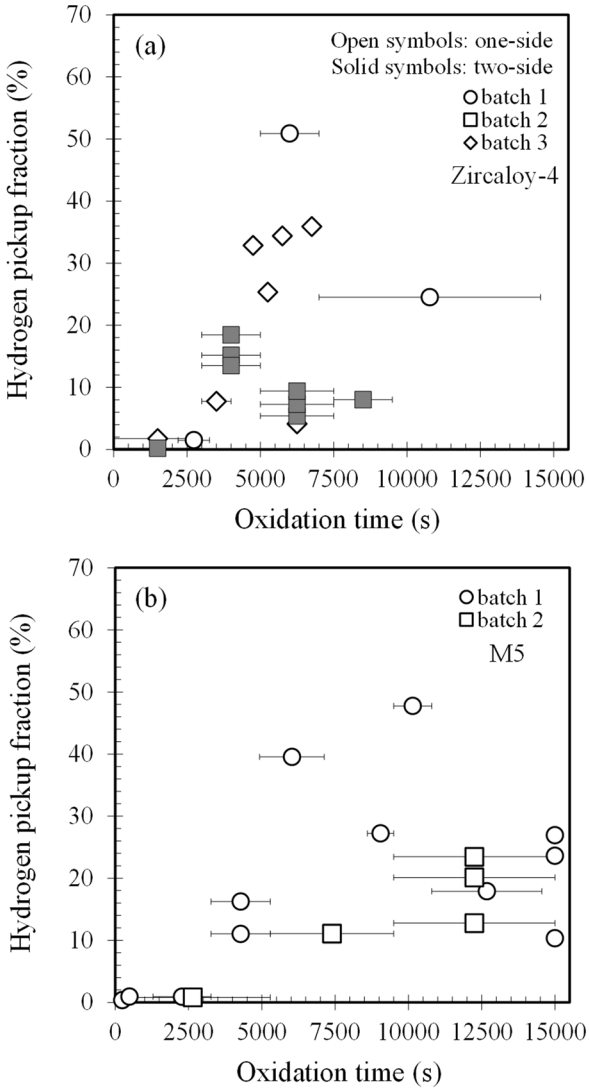

Fig. 8. Evolution of the "instantaneous" hydrogen pickup fraction (reduced to the cladding outer surface) as a function of the oxidation time under steam at 1000°C for (a) three batches of Zircaloy-4 one-sided or two-sided oxidized and (b) two batches of $M5_{Framatome}$ one-sided oxidized (horizontal error bars correspond to time ranges over which the hydrogen pickup fraction has been estimated).

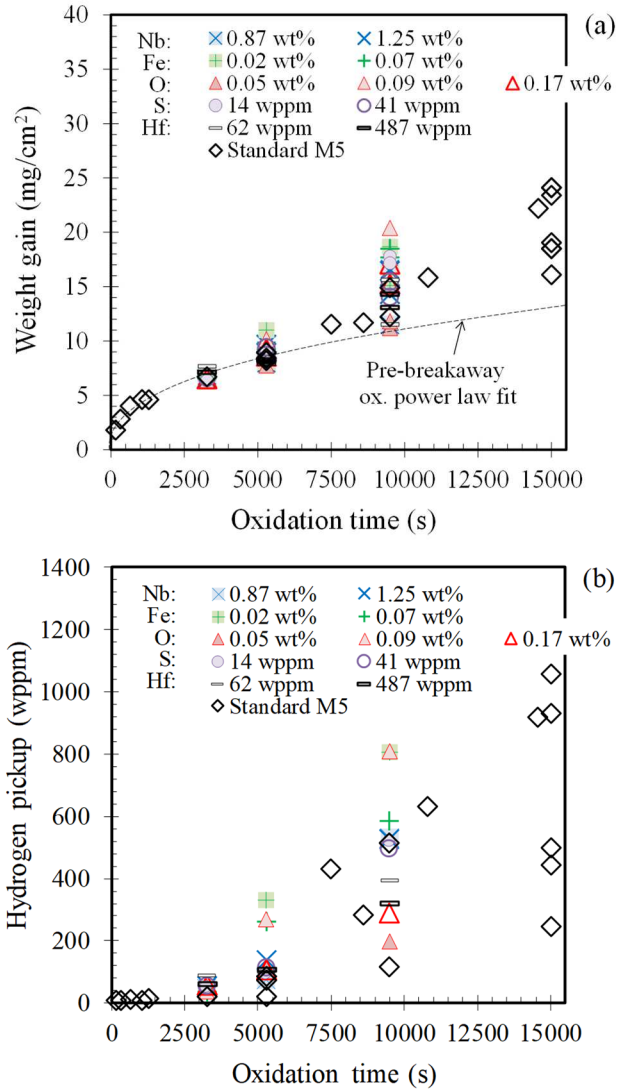

Fig. 9. Evolution of (a) the weight gain and (b) the hydrogen pickup as a function of the oxidation time under steam at 1000°C (one-side oxidation) for standard $M5_{Framatome}$ (batches 1 and 2) and materials with chemical compositions (various contents of Nb, Fe, O, S and Hf) around the nominal specifications of $M5_{Framatome}$.

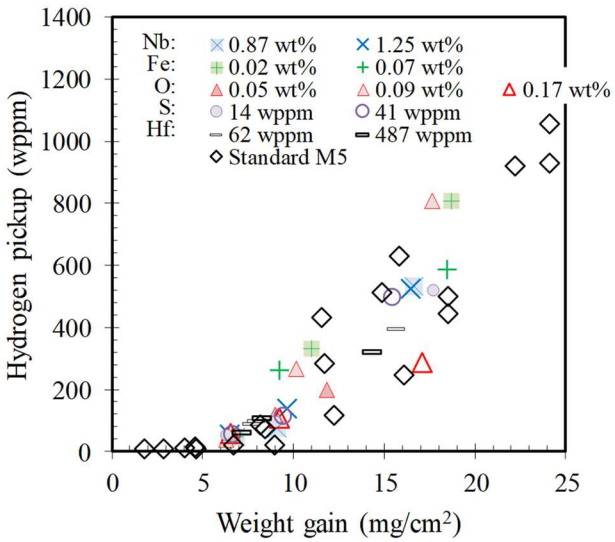

Fig. 10. Evolution of the hydrogen pickup as a function of the weight gain at 1000°C (one-side oxidation) for standard $M5_{Framatome}$ and materials with chemical compositions (various contents of Nb, Fe, O, S and Hf) around the nominal specifications of $M5_{Framatome}$.

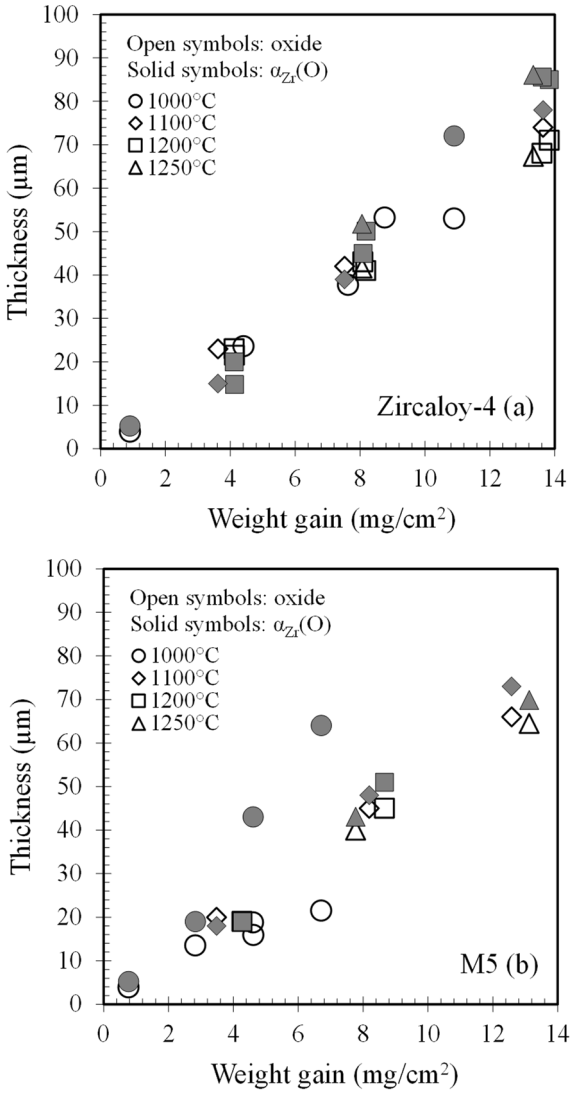

Fig. 11. Thicknesses of the oxide layer and the α_{Zr}(O) layer as a function of the weight gain at 1000°C (before the onset of breakaway oxidation), 1100°C, 1200°C and 1250°C (one-side oxidation) for (a) Zircaloy-4 (batch 1) and (b) $M5_{Framatome}$ (batch 1).

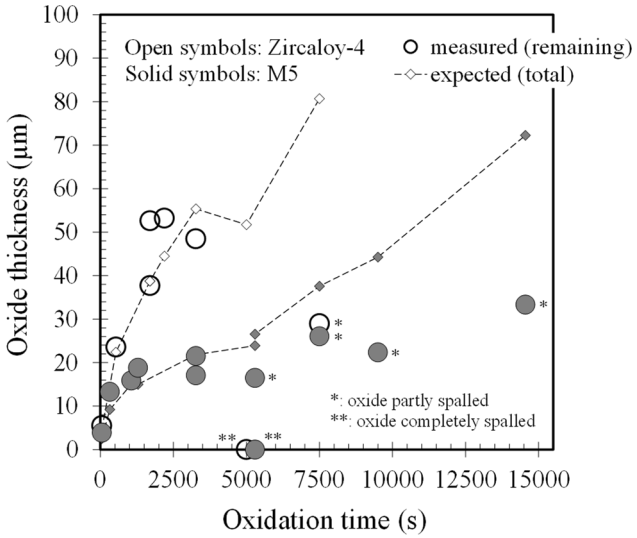

Fig. 12. Evolution of the average oxide thickness remaining at the sample surface after quenching and the total oxide thickness expected from the weigh gain (according to the data shown in Fig. 11), as a function of the oxidation time under steam at 1000°C (one-side oxidation) for Zircaloy-4 (batch 1) and $M5_{Framatome}$ (batch 1).

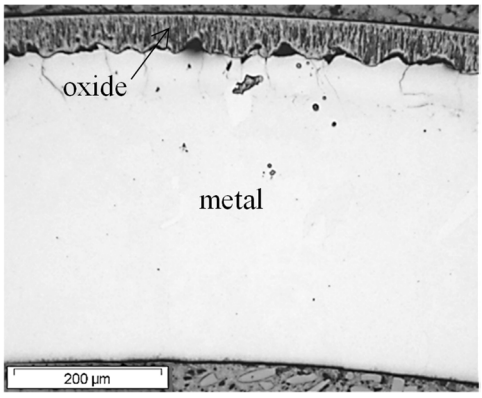

Fig. 13. Optical micrograph of a transverse cross-section of a Zircaloy-4 sample one-side oxidized during 3270 s under steam at 1000°C.

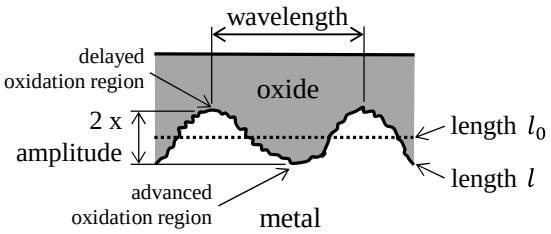

Fig. 14. Schematic representation of the characteristics of the undulations at the metal-oxide interface.

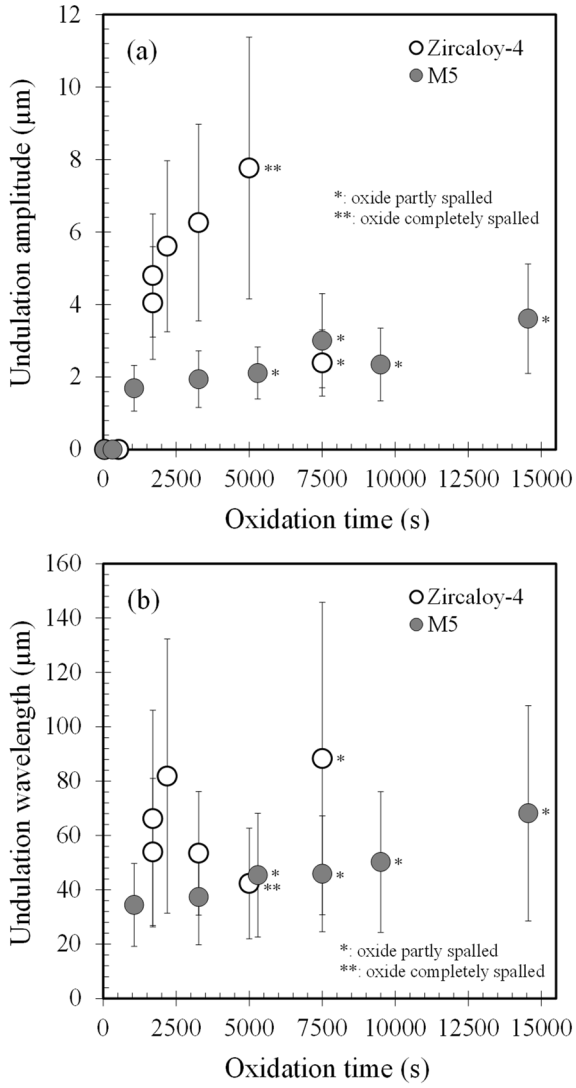

Fig. 15. Evolution of (a) the amplitude and (b) the wavelength of the undulations at the metal-oxide interface as a function of the oxidation time under steam at 1000°C (one-side oxidation) for Zircaloy-4 (batch 1) and $M5_{Framatome}$ (batch 1).

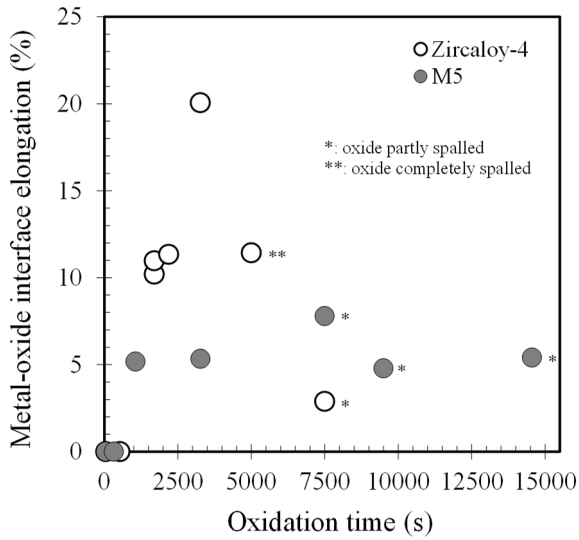

Fig. 16. Evolution of the elongation of the metal-oxide interface due to undulation as a function of the oxidation time under steam at 1000°C (one-side oxidation) for Zircaloy-4 (batch 1) and $M5_{Framatome}$ (batch 1).

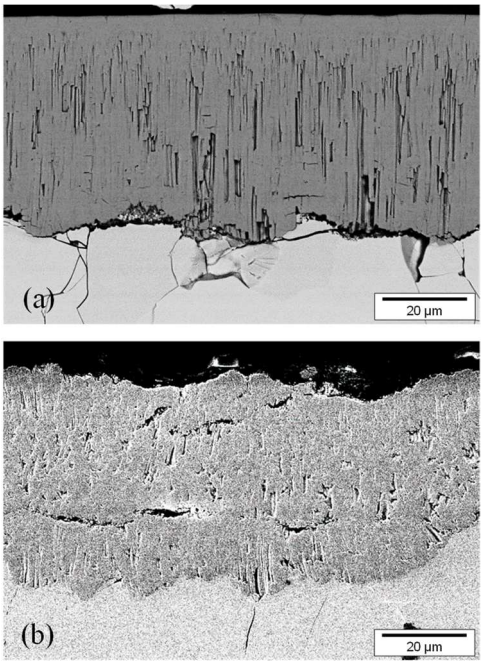

Fig. 17. FEG-SEM micrographs of transverse cross-sections of samples one-sided oxidized at 1000°C and water quenched: (a) Zircaloy-4 (batch 1) oxidized 2193s, (b) $M5_{Framatome}$ (batch 1) oxidized 14551s (outer part of the oxide layer spalled and therefore not visible).

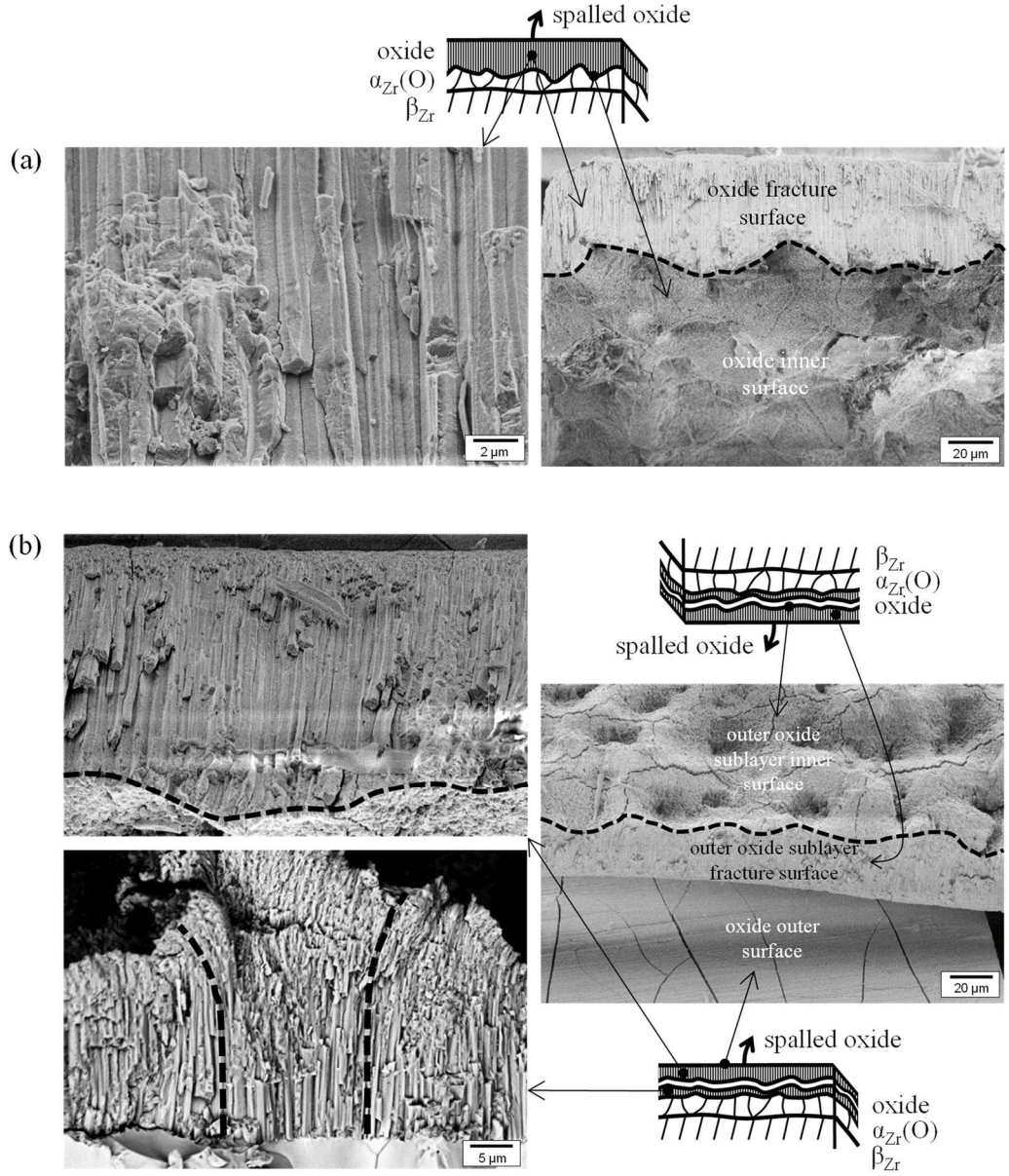

Fig. 18. FEG-SEM fractographs of fragments of oxide spalled during quenching or Zircaloy-4 (batch 1) samples fractured at room temperature after one-side oxidization for (a) 5000 s and (b) 7500 s at 1000°C and water quenching.

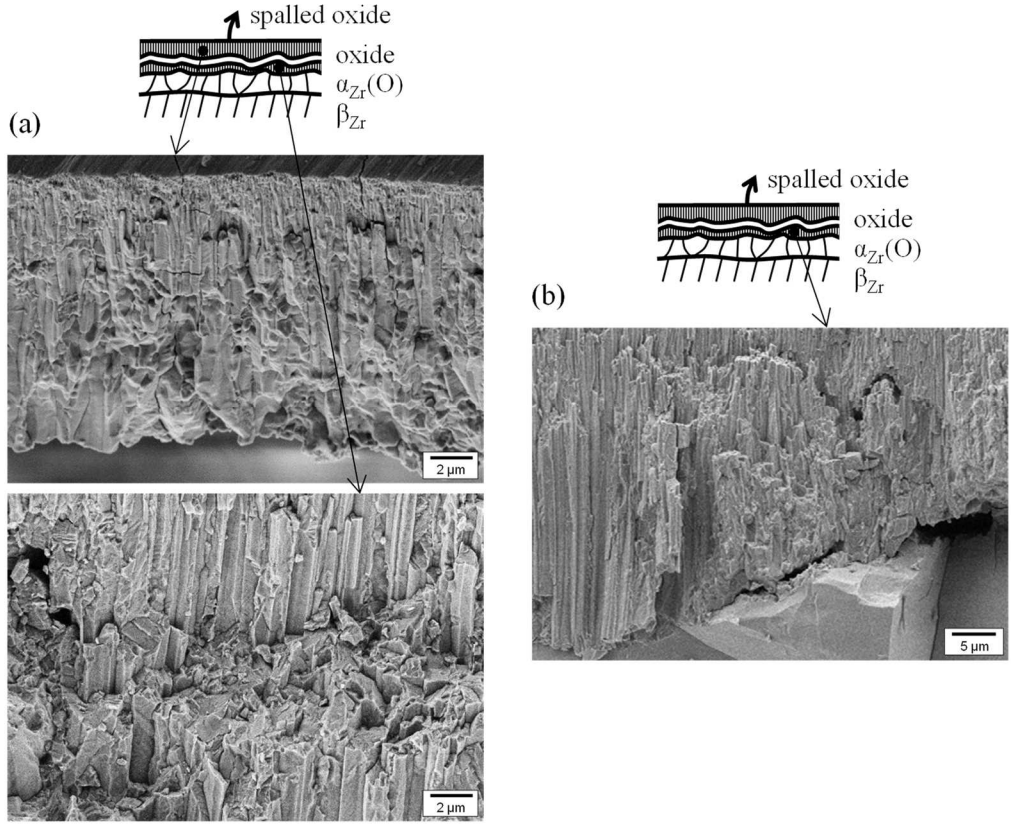

Fig. 19. FEG-SEM fractographs of fragments of oxide spalled during quenching or $M5_{Framatome}$ (batch 1) samples fractured at room temperature after one-side oxidization for (a) 9500 s and (b) 14551 s at 1000°C and water quenching.

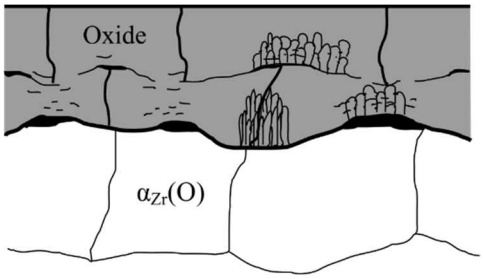

Fig. 20. Schematic representation of the cross-section of the material quenched after breakaway oxidation under steam at 1000°C.

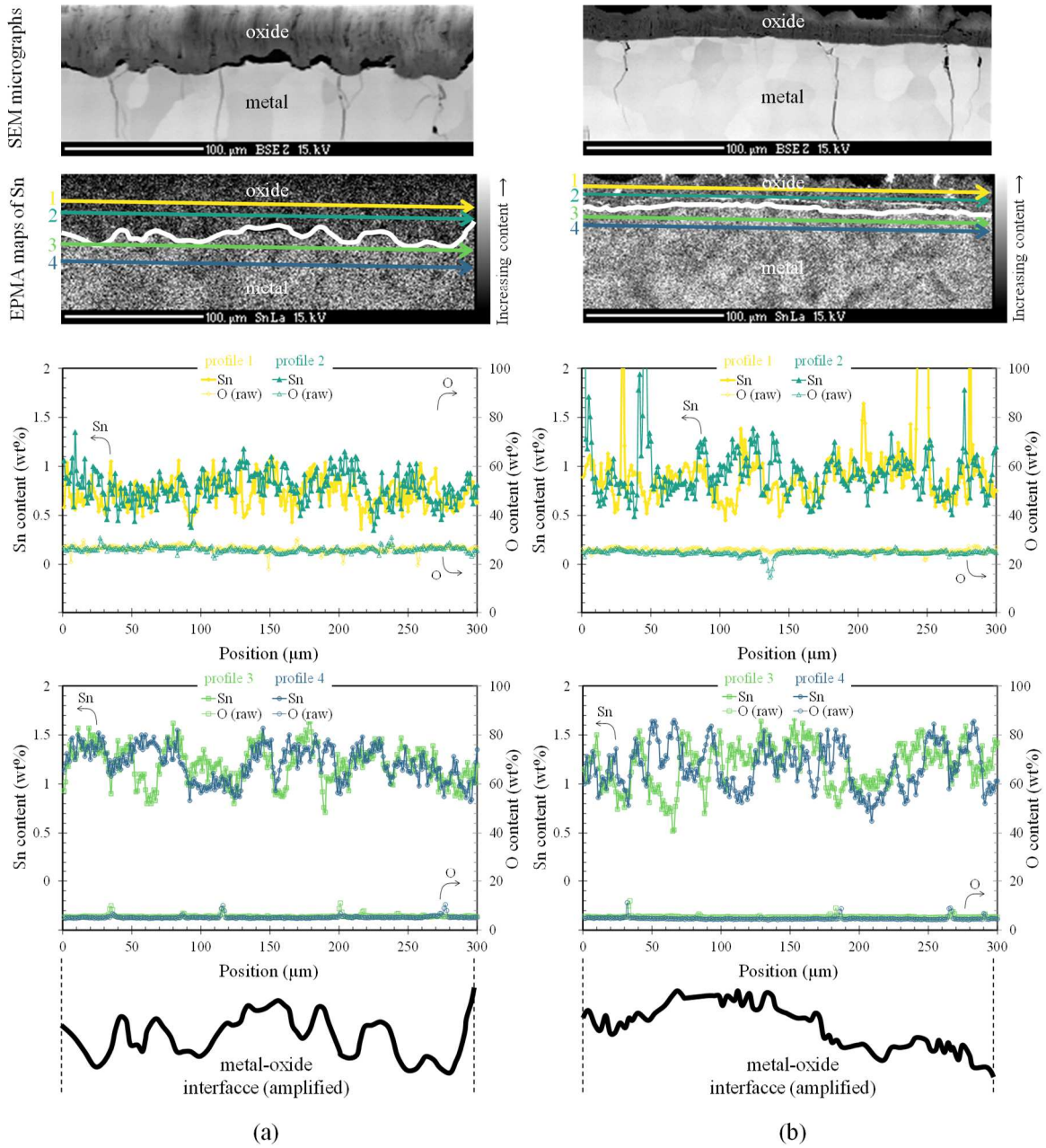

Fig. 21. SEM micrograph, EPMA X-ray map of tin (1 pixel/µm spatial resolution) and tin and oxygen concentration along the profiles numbered 1, 2, 3 and 4 in the map of tin (the raw data reported for oxygen overestimate the actual oxygen content values due to surface contamination which was not corrected here) along the tube hoop direction within the oxide and the metallic substrate, at a few microns from the metal-oxide interface, within Zircaloy-4 (batch 1) samples (one-sided) oxidized for (a) 3270 s and (b) 7500 s at 1000°C and water quenched.

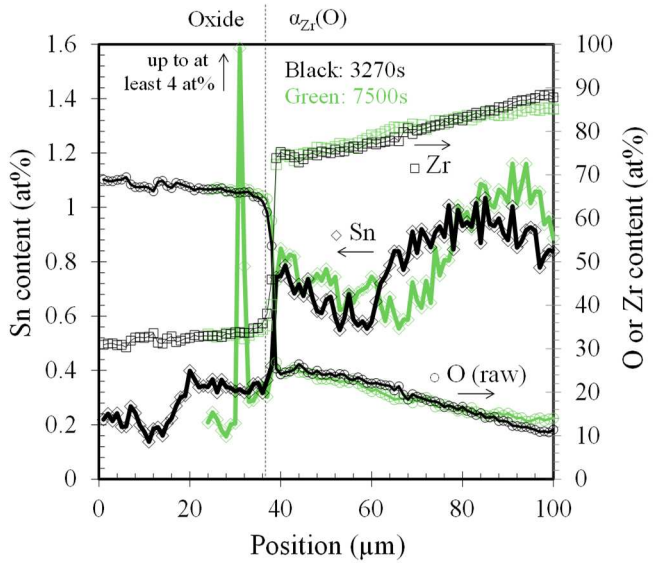

Fig. 22. Concentration profiles of tin, zirconium and oxygen (the raw data reported for oxygen overestimate the actual oxygen content values due to surface contamination which was not corrected here) measured by EPMA along the tube radial direction within the oxide and the metallic substrate within Zircaloy-4 (batch 1) samples (one-sided) oxidized for 3270 and 7500 s at 1000°C and water quenched.

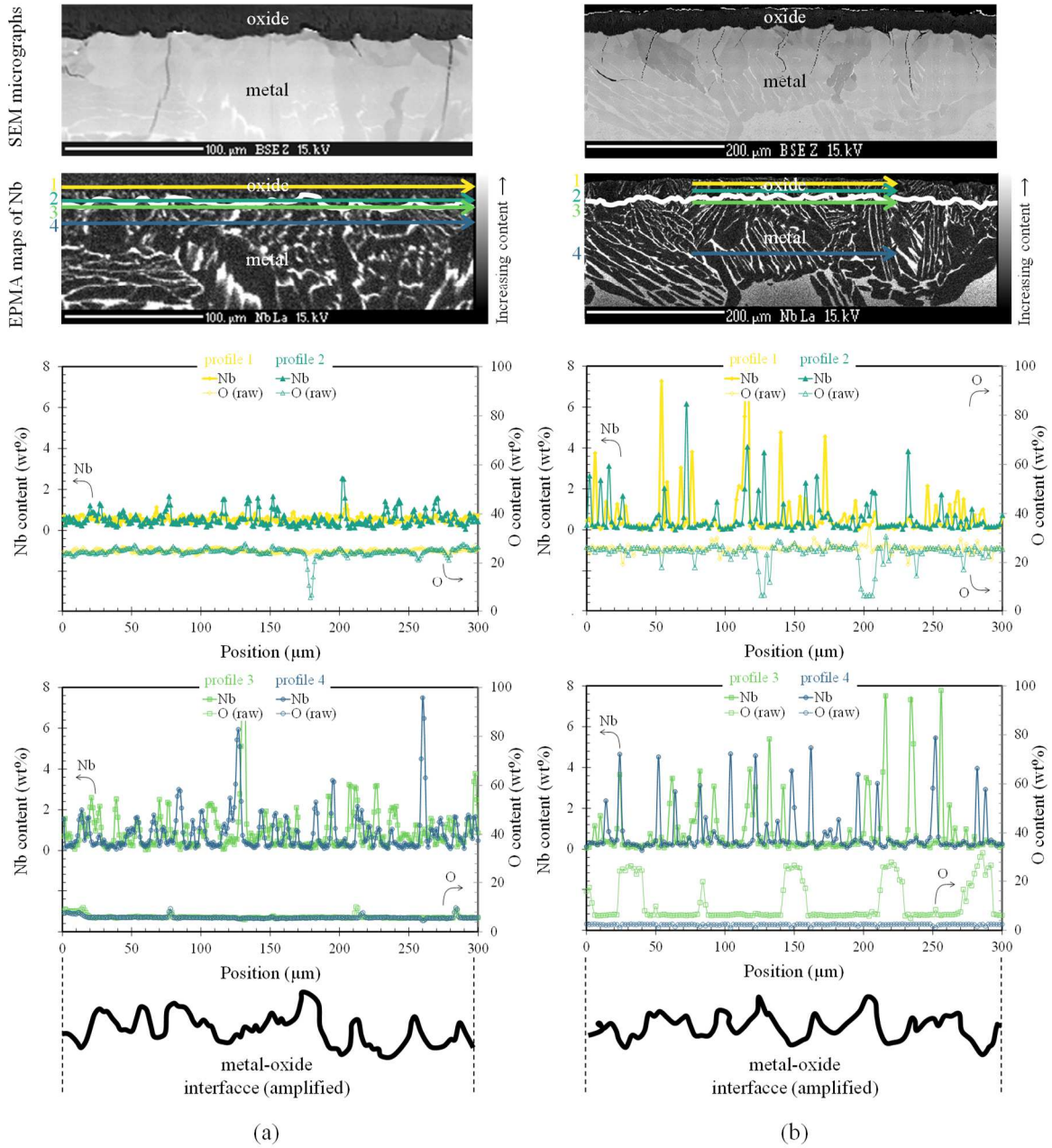

Fig. 23. SEM micrograph, EPMA X-ray map of niobium (1 pixel/µm spatial resolution) and niobium and oxygen concentration along the profiles numbered 1, 2, 3 and 4 in the map of niobium(the raw data reported for oxygen overestimate the actual oxygen content values due to surface contamination which was not corrected here) along the tube hoop direction within the oxide and the metallic substrate, at a few microns from the metal-oxide interface, within a $M5_{Framatome}$ (batch 1) samples (one-sided) oxidized for (a) 3270 s and (b) 7500 s at 1000°C and water quenched.

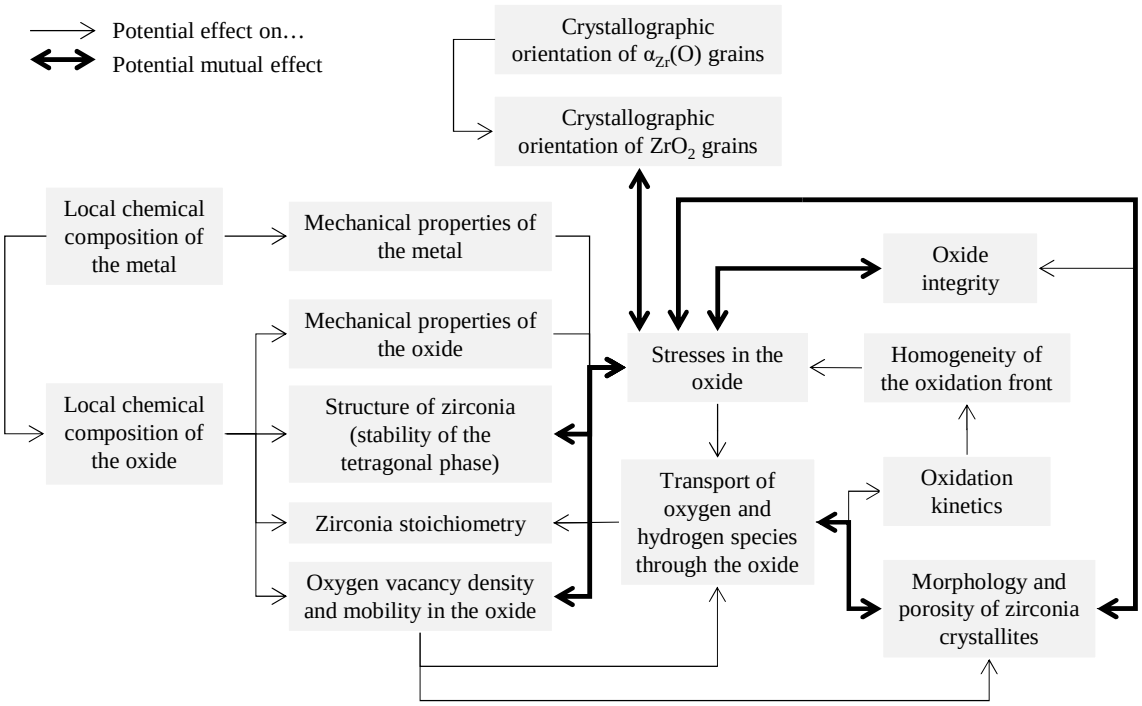

Fig. 24. Factors and properties that may have an effect on breakaway oxidation around 1000°C and potential relationships between them.

Table 1
Nominal chemical compositions of the studied materials (n.c.: not communicated).

	Sn (wt%)	Fe (wt%)	Cr (wt%)	Nb (wt%)	O (wt%)	S (wppm)	Hf (wppm)	Zr
Zircaloy-4	1.3	0.2	0.1	-	0.13	21	51	balance
$M5_{Framatome}$	-	0.03	-	1.0	0.14	17	53	balance
M5 high Nb	-	0.02	-	1.25	0.12	8	36	balance
M5 low Nb	-	0.02	-	0.87	0.12	5	36	balance
M5 high Fe	-	0.07	-	1.02	0.16	11	44	balance
M5 low Fe	-	0.02	-	1.00	0.16	14	50	balance
M5 high O	-	0.02	-	0.97	0.17	13	56	balance
M5 low O	-	0.05	-	0.98	0.09	6	58	balance
M5 very low O	-	n.c.	-	n.c.	0.05	n.c.	n.c.	balance
low S / high O	-	0.03	-	1.00	0.17	14	44	balance
high S / low O	-	0.03	-	0.99	0.13	41	42	balance
low Hf	-	n.c.	-	n.c.	n.c.	n.c.	62	balance
high Hf	-	n.c.	-	n.c.	n.c.	n.c.	487	balance